SiC formation by reaction of Si(001) with acetylene: Electronic structure and growth mode

G. Dufour and F. Rochet*
Laboratoire de Chimie Physique, Université Pierre et Marie Curie, 11 rue Pierre et Marie Curie, 75231 Paris, Cedex 05, France

F. C. Stedile
Departamento de Físico-química, Instituto de Química, UFRGS, Av. Bento Gonçalves, 9500 Porto Alegre, Rio Grande do Sul, Brazil

Ch. Poncey
Laboratoire de Chimie Physique, Université Pierre et Marie Curie, 11 rue Pierre et Marie Curie, 75231 Paris Cedex 05, France

M. De Crescenzi and R. Gunnella
Dipartimento di Matematica e Fisica, Unità dell'Istituto Nazionale di Fisica della Materia, Università di Camerino, 62032 Camerino, Italy

M. Froment
Laboratoire de Physique des Liquides et Électrochimie, Université Pierre et Marie Curie, Tour 22, 4 place Jussieu, 75230 Paris Cedex 05, France

(Received 31 March 1997)

The carbonization process of a single domain 2×1-reconstructed Si(001) vicinal surface (5° off axis from [001] in the [$\bar{1}$10] direction) in acetylene has been studied by combining *in situ* surface science techniques (x-ray photoemission spectroscopy, x-ray photoelectron diffraction, reflection-electron energy loss spectroscopy, low-energy electron diffraction) and *ex situ* analytical techniques (^{12}C and ^{2}H dosing by nuclear reaction analysis, scanning electron microscopy, and reflection high-energy electron diffraction). It is found that at a growth temperature of about 820 °C a variety of growth mechanisms can be observed, particularly during the first step of carbonization. An analysis of C 1*s* and Si 2*p* core-level shifts and of the respective intensities of them, combined with the examination of photoelectron diffraction curves, gives evidence for a penetration of C atoms into the silicon substrate, to form a nonstoichiometric compound. Contemporaneously 3C-SiC nuclei form, aligned with respect to the substrate. Then a quasicontinuous 3C-SiC film grows heteroepitaxially (''cube on cube'' unstrained growth) on the substrate up to a thickness of $\sim$40 Å. C 1*s* and Si 2*p* photoelectron diffraction patterns, compared with calculated ones, show that the single domain initial surface does not necessarily force a preferential alignment of one of the two inequivalent SiC{110} planes with respect to the (110) Si plane. Consequently, such vicinal Si(001) surfaces are not necessarily templates, as often reported in the literature, for the growth of crystalline films free of antiphase boundary domains. Finally, we have observed that an imperfect coalescence of 3C-SiC nuclei leaves easy paths for Si out migration from the substrate and SiC polycrystalline growth, even at a temperature as low as 820 °C. The current models of Si(001) carbonization are examined and compared to our experimental findings. Especially for the very beginning of carbide formation, a unified picture is lacking, as the role played by the steps and terraces of the initial surface remains unclear. [S0163-1829(97)01931-0]

I. INTRODUCTION

Since the pioneering works of Yoshinobu and co-workers[1,2] on acetylene adsorption on Si(111) and Si(001), there is a continuous interest in the surface science community for studying the interaction of small π-bonded hydrocarbons with silicon surfaces, both at experimental[3–9] and theoretical levels.[10–12] In particular, the thermal decomposition steps of acetylene, molecularly chemisorbed at cryogenic temperature on Si(001), have been followed by high-resolution electron energy-loss spectroscopy[2,7]—a vibrational spectroscopy—and thermally programmed desorption.[5,7] A common scenario emerges from these experiments, although some interpretations may differ. Above 530 °C, most of the acetylene molecules remain on the surface and undergo dissociation. At 660 °C, all the hydrogen has left the surface (under the form of H_2 molecules) and carbon atoms bind to silicon atoms. [The behavior of ethylene (C_2H_4) contrasts with that of C_2H_2, although it is also a π-bonded hydrocarbon: most of the molecules desorb intact from the surface at 330 °C.[5]] However, the above-mentioned experimental techniques do not allow a detailed understanding of how C penetrates into the substrate. It is clear that the need for more fundamental research proceeds from the fact that these molecules can be carbon sources for the heterogrowth of silicon carbide on silicon substrates.

Indeed, silicon carbide is a wide-gap (about 2.35 eV) semiconductor, and thus it is a potentially important material for fabricating heterobipolar transistors (HBT).[13] Until now, the conventional approach to the growth of 3C-SiC crystalline films on Si was the chemical vapor deposition (CVD) technique, carried out at high temperature, in the range of

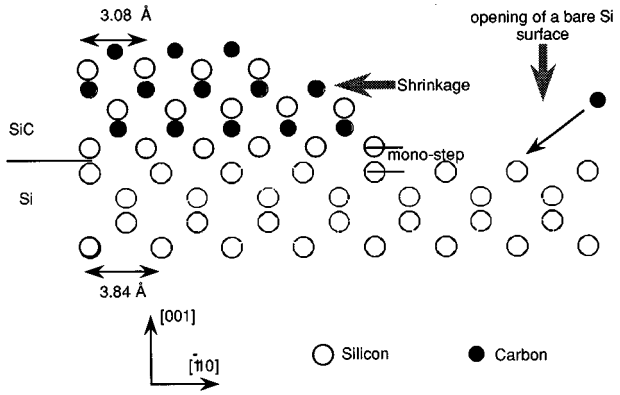

FIG. 1. Schematic picture of the ''⟨110⟩ shrinking row model'' after Ref. 26 [projection in the (110) plane].

1200–1400 °C:[14–16] propane (a saturated hydrocarbon) and silane are cracked at the same time over the Si surface, after the growth of a ''buffer'' layer by direct thermal carbonization in propane.[17,18] This route becomes clearly impractical for HBT fabrication as dopant redistribution in the silicon substrate during thermal treatments must be avoided. Consequently, processing temperatures have to be reduced below 1000 °C. Insofar as the reaction probability of unsaturated hydrocarbons on Si at moderate temperatures is much higher than that of saturated hydrocarbons,[19] SiC thermal growth in acetylene[20–22] and ethylene[23–25] has been the subject of many works. (Note that SiC growth rate obtained by C_2H_2 gas is larger than that obtained by C_2H_4 gas.[19])

According to Bozso *et al.*,[23] stoichiometric SiC grows at temperatures higher than 670 °C. At such temperatures, as already mentioned, hydrogen leaves the silicon surface and C atoms remain. Consequently, the molecular-dynamics simulation of Kitabatake, Deguchi, and Hirao[26] where the starting configuration consists of a layer of C atoms placed over a Si(001)-1×1 surface, provides reasonable scenarios for the growth of 3C-SiC on Si. According to the simulation, two possible mechanisms can occur. In the first scenario, adsorbed C atoms break Si-Si backbonds in the upper layers, thereby allowing Si atomic row spacing to shrink along ⟨110⟩ directions in order to accommodate the Si-C bond length, which is 20% shorter than the Si-Si bond. This is the so-called ''*shrinking Si⟨110⟩ row model*,'' which leads to a locally abrupt SiC/Si interface. A schematic picture of this model is given in Fig. 1. In the second scenario, C atoms can diffuse into the silicon network, destroying the Si lattice on their way in. This suggests that ''$Si_{1-x}C_x$ *alloy*'' phases could form, although, according to the silicon-carbon phase diagram,[27] stoichiometric SiC is the only thermodynamically stable compound. The latter point would be all the more likely because the lower growth temperature reduces kinetics phenomena on the surface.

Both 3C-SiC and GaAs have a zinc-blende structure and grow on Si(001) with the relationship: $[001]_{epilayer} \| [001]_{Si}$ and $\langle 110 \rangle_{epilayer} \| [110]_{Si}$. So, by analogy with the GaAs/Si case, it is believed that stepped Si surfaces[28–30] should facilitate, under high-temperature conventional CVD conditions, the epitaxial growth of 3C-SiC *single-crystal films*, eliminating antiphase boundary (APB) domains. Indeed, Si(001) vicinal surfaces (cut more than 2° off the [001] axis, towards the [110] direction) are known to form a regular array of double atomic-height steps (bisteps) and *single 2×1 reconstructed surface domain* terraces. However, the analogy with GaAs epitaxy on Si(001) is not fully significant. As atoms cap the outermost Si plane of the initial terraces in the GaAs/Si(001) epitaxy, and growth can proceed by the alternate deposition of Ga and As. In the case of SiC growth on Si, there is no reason to imagine that the outermost Si plane of the single domain terraces is systematically terminated by a layer of carbon. C indiffusion in the Si lattice can lead to uneven carbonization depths, and thus to APB's. Again the shrinking ⟨110⟩ row mechanism, although leading to an abrupt Si/SiC interface, will create silicon single atomic-height steps (monosteps), as clearly shown in Fig. 1, when a receding Si row leaves a bare Si surface, with silicon bond directions rotated by $\pi/2$ with respect to those of the shrunk row. This will in turn favor APB formation, unless there is a strong asymmetry in the shrinking direction. Such a growth mode should exist in special growth conditions (that is a preferential shrinking perpendicular to the initial bistep direction): an APB free SiC film was obtained by Kitabatake and Greene[31] after the appropriate carbonization step of a vicinal Si(001) surface, cut 4° off the [001] axis towards [110], with a combination of acetylene gas and solid carbon source. However, Stoemenos *et al.*[32] have shown that the high-temperature CVD deposition on off-axis substrate does not necessarily succeed in eliminating APB's.

In this study we have exposed a vicinal Si(001) surface (cut 5° off the [001] axis towards [110]) to acetylene in a temperature range of 820–900 °C. However, we report here essentially on the reaction of acetylene with silicon at 820 °C. Indeed, exposures at temperatures higher than 880 °C led to the rapid formation of a continuous SiC film, with characteristic square-shaped voids in the Si substrate, that were clearly evidenced by scanning electron microscopy. These macroscopic defects are well-known, and Li and Steckl have given an explanation for their appearance.[18] On the other hand, by lowering the temperature to 820 °C, we were able to follow a variety of phenomena in relation with the chemistry of silicon and carbon and the growth mode of SiC. The choice of a vicinal surface derives from the above considerations about the role that single domain Si surfaces may play on SiC single-crystal growth. The carbonization process was studied *in situ* by various surface techniques: low-energy electron diffraction (LEED), reflection electron energy loss spectroscopy (REELS), x-ray photoemission spectroscopy (XPS), and x-ray photoelectron diffraction (XPD). The present work can be thus compared to previous surface studies on silicon carbonization, where XPS/REELS (Ref. 23) (carbonization in C_2H_4) or XPS/XPD (Ref. 33) (carbonization in activated CH_4) were also used to give information on the chemistry and growth kinetics. By itself XPS is certainly a very powerful tool to characterize the chemistry of the surface. However, the estimation of the growing film thickness means that (i) the film is continuous and has a constant thickness and (ii) that the photoelectron escape depths in the substrate and in the film are known. If these requirements are not fulfilled [in particular point (i)], growth kinetics obtained from XPS measurements become unreliable. This is why complementary *ex situ* characterizations were also carried out: nuclear reaction analysis (NRA) to measure the amounts of fixed ^{12}C (and eventually

the amount of deuterium, when C_2D_2 gas is introduced); scanning electron microscopy (SEM) to follow the morphology of the growing layers; and finally reflection high-energy electron diffraction (RHEED) to determine the film crystallography.

We have evidenced an initial growth regime, up to a thickness of about 40 Å, leading to a quasicontinuous 3C-SiC film aligned with the substrate (twinning is also present). The main observation is that the initial array of bisteps and terraces is immediately destroyed by the carbonization process, as shown by LEED. Contemporaneously C atoms penetrate into the silicon lattice to form a nonstoichiometric compound, as shown by a detailed XPS core-level shift analysis. However XPD curves show that C atoms, which entered into the Si substrate, likely maintain a sp^3 configuration. A long-range-order probe like RHEED points also to the nucleation of $3C$-SiC crystallites. Then SiC growth proceeds until the quasicoalescence of the nuclei. Experimental XPD curves compared with calculated ones confirm the absence of preferential orientation of one of the two nonequivalent SiC{110} planes with respect to the initial silicon surface bistep direction, which is naturally detrimental for APB elimination. Consequently, the asymmetric ''shrinking row'' mechanism of Kitabatake and Greene cannot be applied in all generality to the carbonization of the vicinal surfaces. In the present temperature and pressure conditions, we have never observed the formation of a pure Si top layer floating over the carbide layer.[23,33] On the other hand, pure carbon forms at the growth surface: this carbon layer may have been ignored until now, because of insufficient C $1s$ resolution[23] or contamination by hydrocarbons after reexposure to air before XPS measurements.[22] Finally a second growth regime, under which polycrystalline SiC forms at easy paths for silicon diffusion—as shown by RHEED and SEM—succeeds to the former one, although XPD curves continues to evidence a textured growth.

II. EXPERIMENT

A. Silicon surface preparation and carbonization

Phosphorus-doped wafers (resistivity in the range of 0.002–0.005 Ω cm) purchased from SILTRONIX SA, miscut by 5° towards [110] off the [001] axis, were cleaned by flashing directly the wafer for 10 s at 1100 °C by Joule heating in an ultrahigh vacuum preparation chamber (base pressure mid 10^{-10} Torr range). Temperatures were measured with an infrared pyrometer. After cooling down to room temperature, single domain 2×1 patterns were observed by LEED. The successive carbonization steps of a silicon wafer were carried out at 820 °C and under pressures of acetylene in the 5×10^{-7}–5×10^{-6} Torr range. Acetylene pressures were measured with a ionization gauge whose reading was corrected by a sensitivity factor of 2 [the sensitivity factor is 1 for N_2 (Ref. 34)]. The exposures Q are given in molecules/cm^2 using the relation $Q=(P\times t)/\sqrt{2\pi m k_B T}$, where P is the pressure, t the dose time, m the mass of the molecule, k_B the Boltzman constant, and T the room temperature.[35] During all acetylene exposures the sample was cooled down to room temperature while still in acetylene. After each carbonization step, the gas was pumped down, and the sample was directly transferred into the analysis chamber, without breaking the UHV conditions, where XPS/XPD and REELS measurements were made. To get further insights into the role of hydrogenated species during carbide formation, several Si wafers were treated in 99%-enriched C_2D_2 gas in order to perform subsequent *ex situ* NRA. As a matter of fact, exposure of the sample to air precludes any reliable *ex situ* dosing of ^{1}H hydrogen, as the surface will be covered by hydroxylated species. After ^{12}C and D dosing by NRA, the crystallinity of the grown layers was investigated by RHEED, and their morphology was studied by SEM.

B. X-ray photoemission

The x-ray photoelectron spectra of core levels (Si $2p$, C $1s$) and of the valence band have been obtained with a nonmonochromatized Mg $K\alpha$ source ($h\nu=1253.6$ eV), operating at an anode voltage of 15 kV and an emission current of 20 or 30 mA. The hemispherical analyzer is a KRATOS XSAM800, operating in the so-called ''fixed analyzer transmission mode,'' with a pass energy of 40 eV. The energy resolution in this case is such that the full width at half maximum of the Ag $3d_{5/2}$ line is 1 eV. The binding-energy scale is calibrated from the Au $4f_{7/2}$ line at 84 eV. Angle-resolved Si $2p$ and C $1s$ spectra have been also recorded, with the [110] step edge direction either parallel or orthogonal to the analyzing plane defined by the direction of the incident photons and that of the emitted electrons, these two directions making a fixed angle of 60°. The experimental geometry is given in Fig. 2. In the following, polar scans parallel and orthogonal to the [110] step will be called ''para'' and ''ortho,'' respectively. The polar angle θ is varied by rotation of the sample holder around an axis perpendicular to the analyzing plane. In the ''ortho'' geometry the scans are performed in the (110) silicon plane: θ_{ortho} is equal to zero when the crystal [001] direction is aligned with the analyzer axis and is positive when the analyzer looks from upstairs. In the ''para'' geometry, the scans are performed in the plane defined by the normal to the optical plane **n** and the [110] direction. Then, θ_{para} is equal to zero when the analyzer axis is parallel to **n** (**n** is then inclined by 5° downstairs from [001]). The electron acceptance of the electrostatic lens is not specified by the manufacturer. However, polar angle features of full width at half maximum (FWHM) of less than 5° have been observed on clean reconstructed Si(001)-2×1 surfaces. The angle resolution is thus comparable to that of Ref. 36. XPS data treatments are carried out as follows. A Shirley background is subtracted[37] from the raw C $1s$ and Si $2p$ spectra. For clarity, the Si $2p_{1/2}$ component of the Si $2p$ doublet is numerically stripped assuming a spin-orbit distance of 0.6 eV and $2p_{1/2}/2p_{3/2}$ branching ratio of 0.5.[38] The experimental curves are fitted with sums of Gaussians convoluted with Lorentzians which have fixed FWHM equal to 0.3 eV. This latter value is not the core-hole lifetime broadening which is much smaller,[39] but simply accounts for the form of the instrumental function when one uses a nonmonochromatized Mg $K_{\alpha1,2}$ line. The XPD polar curves are taken with angular steps of 2.5°. For each angular position the Si $2p$ and C $1s$ spectra are recorded and after background subtraction, the peak area is measured. Curve fitting, when it

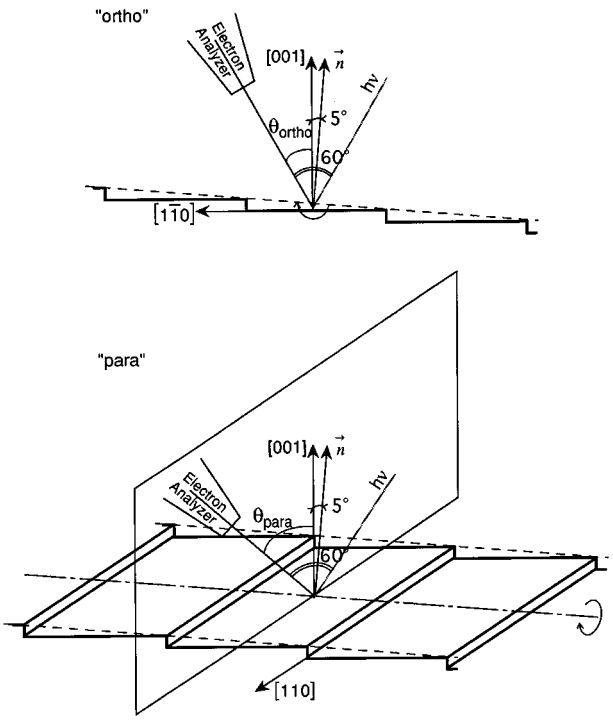

FIG. 2. XPS/XPD experiments in the ''ortho'' and ''para'' geometries. In ''ortho'' geometry the analyzing plane is perpendicular to the [110] step edge direction and contains the [001] direction: then the polar angle θ_{ortho} is measured from the [001] axis. In ''para'' geometry the analyzing plane is parallel to the step edge direction, the [001] axis is 5° off (upstairs) and thus θ_{para} is measured from the normal to the optical plane **n**. The angle between the incidence of light and the analyzer axis is constant and equal to 60°. In all geometries **n** belongs to the analyzing plane.

makes sense, is also used to separate the various chemical contributions, whose intensity variations are then plotted versus θ.

C. REELS

Electron energy losses are measured in reflection geometry. The primary beam makes an angle of 60° with **n**, which is aligned with the spectrometer axis ($\theta=0°$). A pass energy of 10 eV is used, such that the elastic peak FWHM is 0.46 eV. Reducing the primary beam energies E_p from 1000 to 100 eV, the electron penetration depth (and hence the probed thickness) decreases from $\sim$20 Å to about $\sim$5 Å.[40]

D. Complementary ex situ characterizations

The nuclear reaction $^{12}C(d,p)^{13}C$ induced by 970 keV deuterons at $\theta_{\text{lab}}=150°$, a Ta_2O_5 standard and the $^{16}O(d,p_1)^{17}O$ reaction induced by 850 keV deuterons at $\theta_{\text{lab}}=150°$ are used to measure the absolute number of ^{12}C per cm^2 incorporated in the carbonized film, knowing the amount of ^{16}O in the standard (accurate within $\pm3\%$) and the differential cross-section ratio defined as $R_{C/O}=(d\sigma^C/d\Omega)_{970\text{ keV}}/(d\sigma^O/d\Omega)_{850\text{ keV}}=5.565$ recently measured by Quillet, Abel, and Schott[41] with an accuracy better than $\pm5\%$. The amount of deuterium is measured with the $D(^3He,p)^4He$ reaction induced by a 700 keV $^3He^+$ beam at $\theta_{\text{lab}}=150°$ (Ref. 42) and a *D* containing standard (accuracy $\pm5\%$). The oxygen contamination after exposure to air is controlled using the $^{16}O(d,p_0)^{17}O$ induced by a 850 keV deuteron beam at $\theta_{\text{lab}}=90°$. NRA measurements are averaged on the surface (2×3 mm^2) probed by the ion beam.

SEM images are taken in the so-called ''secondary electron mode.'' RHEED patterns are obtained at grazing incidence with a JEOL 100 CXII microscope operated at 100 kV.

III. RESULTS AND DISCUSSION

A. ^{12}C and D content, morphology, and long-range order

Several samples have been treated in deuterated acetylene at 820 °C (and at 840 °C) in the 0.5×10^{-6}–2.1×10^{-6} Torr range for various lengths of time: the corresponding ^{12}C and D contents, measured by NRA, are given in Table I. We underline that these values are mean values, as the films may not be uniform in thickness, especially for the longest doses (see below). A slight oxidation during the transport in air is measured (about 3×10^{15} O atoms/cm^2). Also carbon contamination adsorbed during the transport, estimated to a few 10^{15} C atoms/cm^2, makes that the carbon content determined for the shortest exposure is an upper limit of what is actually fixed by the carbonization process. At constant pressure ($\sim2\times10^{-6}$ Torr corresponding to a flux of $\sim8\times10^{14}$ molecules cm^{-2} s^{-1}) and temperature ($\sim$820 °C) the growth kinetics follows a rather parabolic law, $X^2=K_pt$ where X is the equivalent SiC thickness obtained from the ^{12}C measurements and t the carbonization duration. The parabolic constant K_p is about 3.3×10^{-15} cm^2 s^{-1} and if we assume, as in Ref. 43, that the mobile species is silicon, we obtain a diffusion coefficient of about 1.6×10^{-15} cm^2 s^{-1} for Si.

TABLE I. ^{12}C and D amounts measured *ex situ* by NRA after thermal carbidization in C_2D_2. Taking the bulk carbon density in 3*C*-SiC (4.83×10^{22} C atoms/cm^3), 10^{15}C atoms/cm^2 correspond to an equivalent thickness of 2.07 Å.

P ($\times10^{-6}$ Torr), T (°C)	Dose (10^{17} molecules/cm^2)	^{12}C amount (10^{15} atoms/cm^2)	D amount (10^{14} atoms/cm^2)
0.5,820	0.25	6.8±0.7	2.1±0.3
2.1,820	1.2	20±2	2.8±0.35
2.1,820	14.8	122±12	4.8±0.5
2.1,820	44.6	199±20	6.1±0.6
2.1,840	59	237±22	4.1±0.5

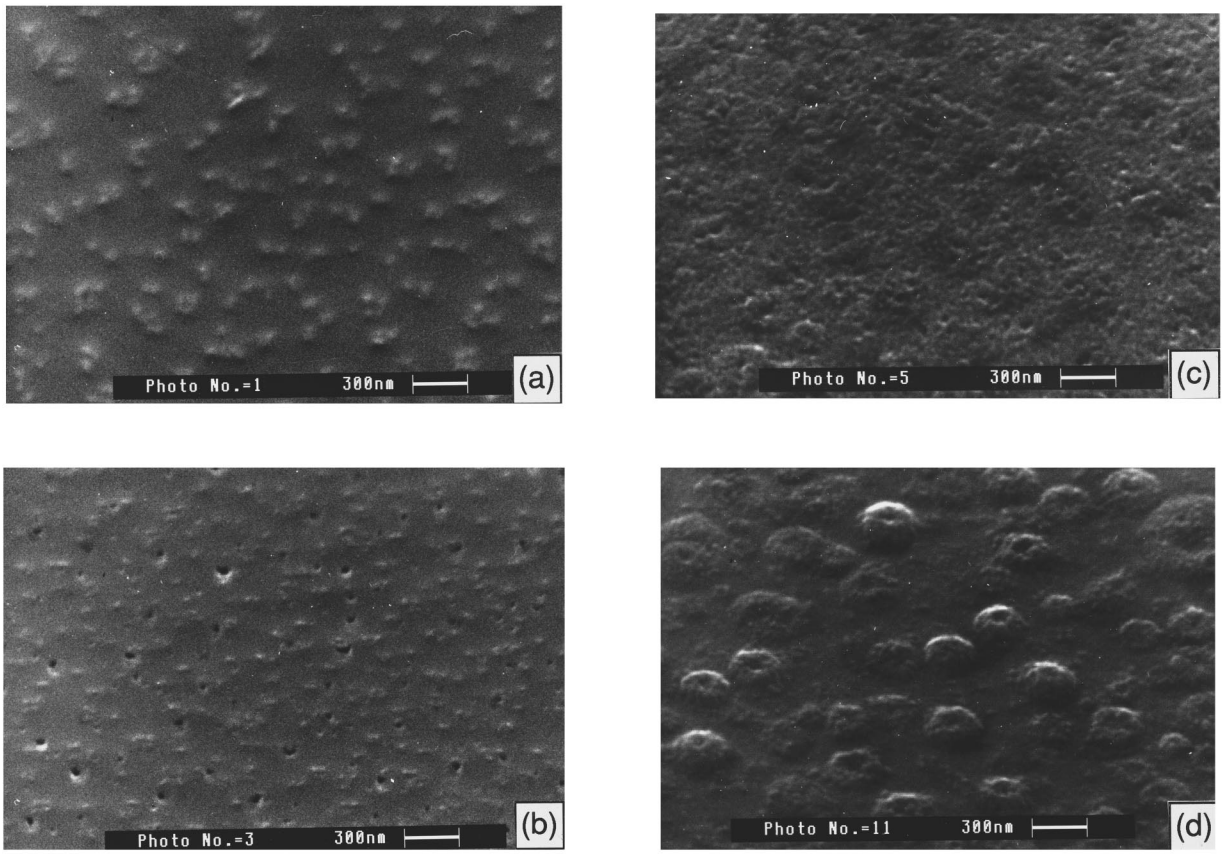

FIG. 3. Scanning electron microscopy (secondary electron mode) at a magnification of 90 000 of carbonized silicon surfaces for various acetylene exposures Q (in 10^{17} molecules/cm^2): (a) 0.25, (b) 1.2, (c) 14.8, and (d) 60. The growth temperature is 820 °C for (a)–(c) and 840 °C for (d). (For the ^{12}C content see Table I.)

We also observe that deuterium is present in C_2D_2-carbonized films, but in extremely small amounts, a few 10^{14} D atoms/cm^2, i.e., a fraction of a monolayer.[44] This content increases slowly with increasing thicknesses at a given reaction temperature. However, the present technique does not allow the reader to know where deuterium is located. If hydrogen remained at the interface between Si and SiC, its amount would be sufficient to passivate eventual broken Si bonds at cores of misfit dislocations: indeed the lattice mismatch between SiC and Si produces misfit dislocations along the Si/SiC interface with a density of 6.5 $\times 10^6$ cm^{-1} (Refs. 17 and 31) along a ⟨110⟩ direction. The passivation of dangling bonds by hydrogen at the interface could also have profound implications in the band alignment of Si/SiC heterostructures.

The SEM images of the carbonized silicon surfaces are presented in Fig. 3. The angle of view is at 45° from the surface normal. Although the fixed carbon amount is rather low ($\leqslant 6.8\times 10^{15}$ atoms/cm^2 or an equivalent thickness of $\sim$14 Å), Fig. 3(a) shows that the surface is far from being featureless. The surface is covered by protuberances with a surface density of $\sim 2\times 10^9$ cm^{-2}. They seem to be conically or pyramidlike shaped, with an average base-diameter of $\sim$400 Å. The presence of 3C-SiC nuclei evidenced by RHEED may be the cause of a strong deformation of the silicon substrate around them. For an exposure of 1.2 $\times 10^{17}$ molecules/cm^2 (carbon content of ~ 20 $\times 10^{15}$ atoms/cm^2, equivalent thickness $\sim$40 Å) [Fig. 3(b)], the contrast of the protuberances is smaller, although their density is much the same as for the previous micrograph. A new feature is the aperture of black ''wells'' with density $\sim 5\times 10^8$ cm^{-2} that are drilled through the surface. For much higher exposures (above 10^{18} molecules/cm^2, equivalent thicknesses $\geqslant$200 Å) the film morphology changes drastically. Volcanoes grow up [Figs. 3(c) and 3(d)] above a flatter surface. Their areal density, which is the same as that of the black wells of Fig. 3(b) suggests that they continue the wells themselves.

The crystalline order of the carbonized layers is examined by RHEED. The diffraction patterns, taken in the silicon ⟨110⟩ azimuth (or close to it), are shown in Fig. 4. For exposures $Q\leqslant 1.2\times 10^{17}$ molecules/cm^2, 3C-SiC diffraction spots and streaks are superimposed on the streaked pattern of the silicon substrate characteristic of the ⟨110⟩ azimuth [Figs. 4(a) and 4(b)]. Positions of the SiC reflections correspond to a ''cube on cube'' alignment with the substrate, following the (nonstrained) heteroepitaxial relationship:

$$\mathrm{SiC}[001]\|\mathrm{Si}[001] \quad \text{and} \quad \mathrm{SiC}[110] \ (\text{or } [\bar{1}10])\|\mathrm{Si}[110].$$

However, the orientation of carbide crystallites is not unique, as twinning is also present [Fig. 4(c)]. Twinning during 3C-SiC growth is indeed frequently observed.[26,31] For the long exposures, which correspond to the volcanolike growth observed by SEM, we obtain ring patterns, characteristic of

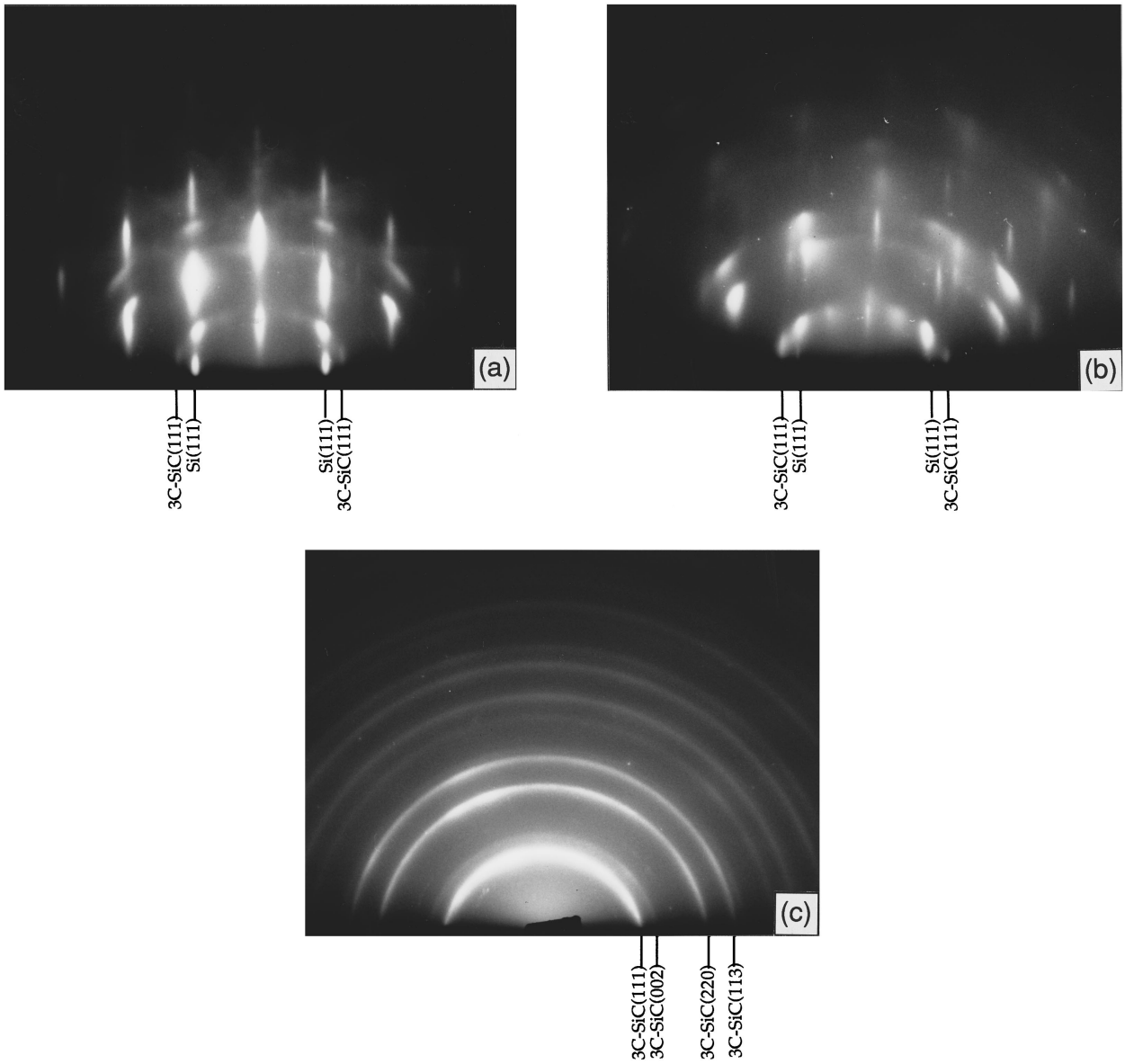

FIG. 4. RHEED patterns taken in the Si [110] azimuth for silicon surfaces carbonized at 820 °C for various acetylene exposures Q (in 10^{17} molecules/cm^2): (a) 0.25, (b) 1.2, and (c) 44.6. (For the ^{12}C content see Table I.)

completely randomly oriented $3C$-SiC microcrystallites. Figure 4(d) shows a pattern typical of such films.

B. Surface crystallography

The clean vicinal surface is characterized by (001) terraces, separated by bisteps whose edges are parallel to the [110] direction. Surface silicon atoms rebond two by two to form dimers, whose rows run perpendicularly to the step edges, giving a *single* 2×1 domain we have observed by LEED [Fig. 5(a)].

After each step of carbonization LEED is used to characterize the surface. For acetylene exposures smaller than $\sim10^{17}$ molecules/cm^2 [Fig. 5(b)], we observe the loss of the half-order spots of the original 2×1 reconstruction and that of the doublet splitting characteristic of a regular bistep array. The LEED patterns contain the nonsplitted integral order spots (those of silicon) and other spots (not the specular spot) that move along the four $\langle110\rangle$ directions when we change the electron-beam energy. This indicates that *four* $\{11n\}$ facets have formed. Facetting may be related to the protuberances observed by SEM [Fig. 3(a)] at the beginning of carbonization. For higher acetylene doses the LEED patterns can no longer be observed.

C. Electronic structure

XPS C $1s$ and Si $2p_{3/2}$ spectra for increasing acetylene exposures Q (in the range 10^{16}–10^{18} molecules/cm^2) at 820 °C are shown in Fig. 6, along with curve reconstructions. Spectra from a thick continuous carbide film grown at 880 °C, termed ''reference SiC'' are also given in Fig. 6 for comparison. The observed binding energy differences of the various structures, as a function of exposure, are given in Fig. 7.

First let us focus on the C $1s$ spectra. We notice its asymmetry for all exposures. Two components can be clearly distinguished: the first one, of FWHM 1.9 eV and spectral

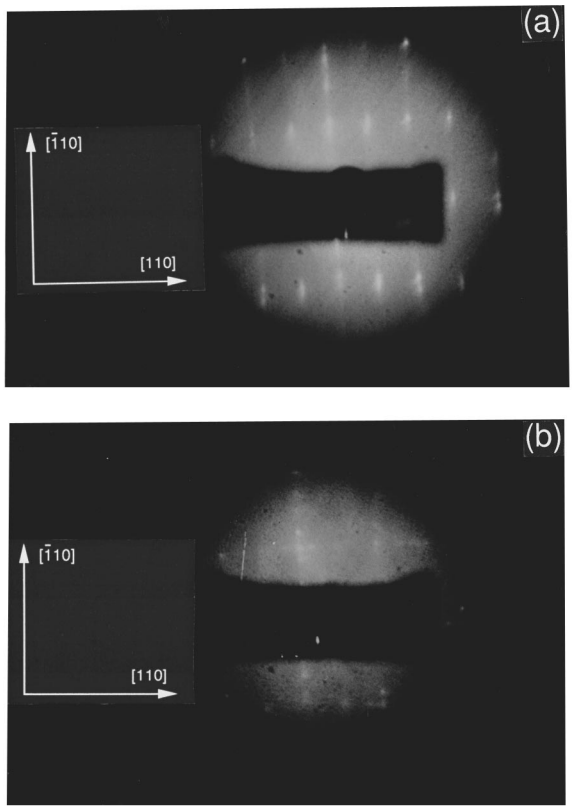

FIG. 5. LEED patterns (72 V) from the Si surfaces inclined by 5° from the (001) plane towards [110]. (a) Clean stepped Si(001) showing a single 2×1 reconstructed surface domain: half order spots due to Si dimerization are observed along [110], a direction parallel to the bistep edges; (b) carbonized Si(001) surface, exposed at 820 °C to an acetylene dose of 3.6×10^{16} molecules/cm^2, showing four symmetric $\{11n\}$ facets.

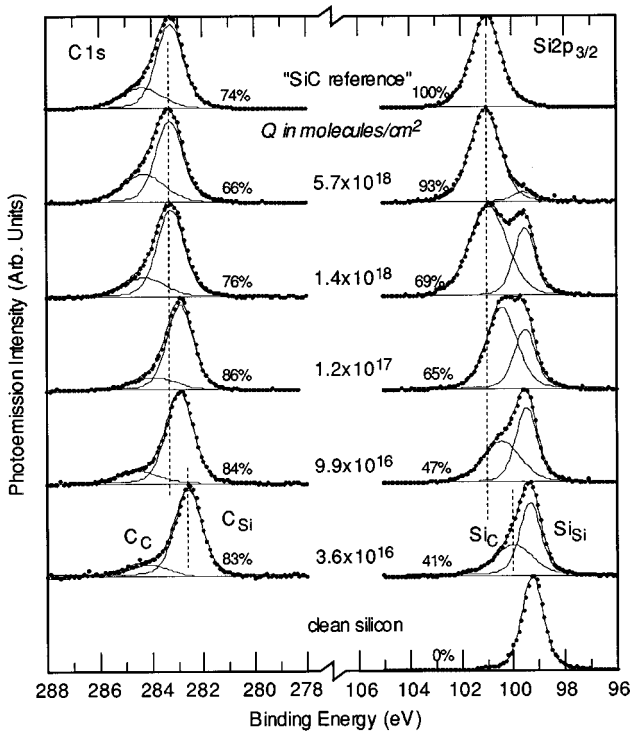

FIG. 6. Nonmonochromatized (Mg $K\alpha$) C 1s and Si $2p_{3/2}$ core-level spectra (dots) of the clean and acetylene-carbonized surface at 820 °C. Q is the acetylene dose. The ''SiC reference'' is a surface exposed at 880 °C to a dose of 6×10^{18} molecules/cm^2. Best fits (solid curves) are also given: the Lorentzian FWHM is 0.3 eV, the Gaussian FWHM is 0.8 eV for Si_{Si} (elemental Si), 1.55 to 1.21 eV for Si_C (Si bonded to C), 1.06 eV for C_{Si} (C bonded to Si), and 1.73 eV for C_C (C bonded to C). The corresponding spectral weights of C_{Si} and Si_C components are indicated in the figure. All spectra are taken at a polar angle (θ_{ortho} or θ_{para}) equal to zero.

weight 14–34 % is clustered at ~284.3 eV, while the other one, of FWHM 1.23 eV is separated from the former by at least 1.2 eV towards lower binding energies. Under the same analysis conditions, we have indeed found C 1s peaked at 284.35 ± 0.05 eV for a highly oriented pyrolytic graphite (HOPG) sample. Hydrocarbon polymers are expected at 284.8 ± 0.3 eV as indicated in Ref. 45 (for a spectrometer tuned to Au $4f_{7/2}=83.95\pm0.05$ eV as in the present work). In view of the very small amount of deuterium detected in the films, it is reasonable to attribute the 284.3 eV peak to carbon bonded to carbon (denoted here C_C) and not to hydrocarbons as reported in Ref. 46. REELS spectra (Fig. 8) give complementary information on the nature of the C-C bond. The spectra of the carbonized Si surface, taken both in bulk- and surface-sensitive conditions, never exhibit the characteristic energy loss of sp^2 carbon at 6.5 eV that shows up for HOPG (upper curves of Fig. 8) and also for the graphitized $3C$-SiC(001)-1×1 surface.[47] This points to the likely formation of a sp^3 bonded pure carbon layer.

The low binding-energy component of C 1s is attributed to the growing carbon-silicon compound (denoted C_{Si}). A comparison with C 1s binding energies of SiC in literature is made difficult, because of the considerable spread of the data [C 1s ranges from 282.3 to 283.6 eV (Ref. 48)], that arises from band bending differences between samples. We observe an increase in the binding energy of C_{Si} from ~282.7 eV (for $Q\leqslant10^{17}$ molecules/cm^{-2}) to ~283.2 eV for the longest exposures (in the 10^{18} molecules/cm^2 range), the latter binding-energy value being the one of the ''reference SiC'' film.

The corresponding Si $2p_{3/2}$ core levels of the films grown at 820 °C present two components. The one at lower binding energy (at ~99.3 eV) and of FWHM 1 eV (denoted Si_{Si}) is a contribution from the silicon substrate, which does not disappear even for the higher doses corresponding to mean NRA thicknesses greater than 400 Å (see Table I). In all cases this contribution is attenuated at glancing photoelectron emission (see below). As we already know from SEM images that the SiC films are extremely inhomogeneous in thickness for the exposures above 10^{18} molecules/cm^2, this means that the gaps between SiC hills (or volcanoes) are zones covered by a thin carbon-silicon compound layer.[49] The other component (denoted Si_C) situated at higher binding-energy is attributed to the compound formed between silicon and carbon. For $Q\leqslant10^{17}$ molecules/cm^2 its FWHM 1.7 eV is larger than for the highest exposures (FWHM~1.4 eV). The binding-energy difference $\Delta_1=$Si $2p_{3/2}(Si_C)-$Si $2p_{3/2}(Si_{Si})$ plotted in Fig. 7(a) increases with increasing Q (from 0.6 to 1.5 eV). But it would be naive to interpret these increasing shifts only in terms of chemical changes in the growing layer as a correlative increase in C $1s(C_{Si})$ binding energies is also observed. The binding-

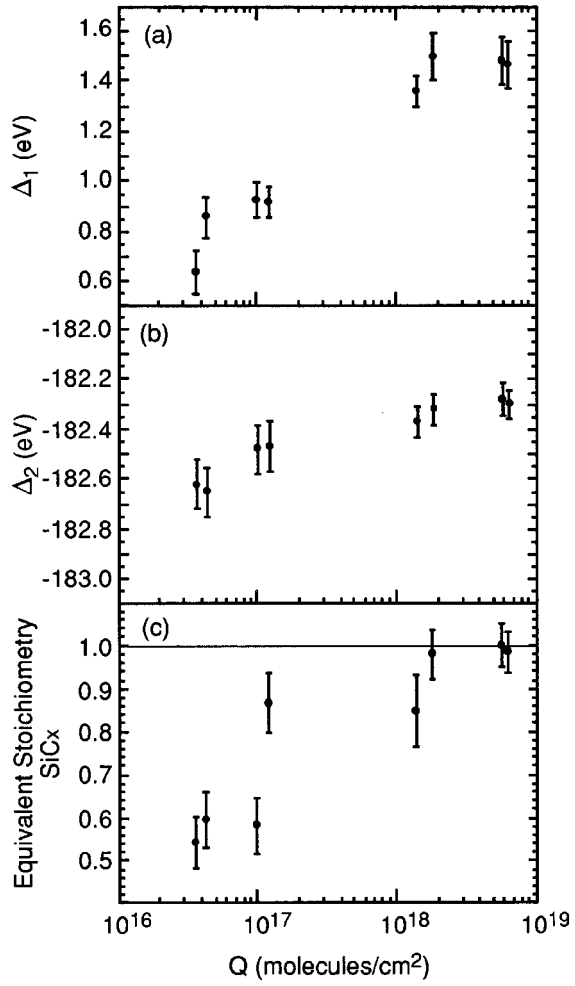

FIG. 7. Variations of $\Delta_1 = \mathrm{Si}\ 2p_{3/2}\ (\mathrm{Si_C}) - \mathrm{Si}\ 2p_{3/2}(\mathrm{Si_{Si}})$ [panel (a)], of $\Delta_2 = \mathrm{Si}\ 2p_{3/2}(\mathrm{Si_C}) - \mathrm{C}\ 1s(\mathrm{C_{Si}})$ [panel (b)] and of the equivalent stoichiometry SiC_x [panel (c)], as a function of the exposure Q ($T = 820\,^\circ\mathrm{C}$), deduced from curve reconstructions of Fig. 6.

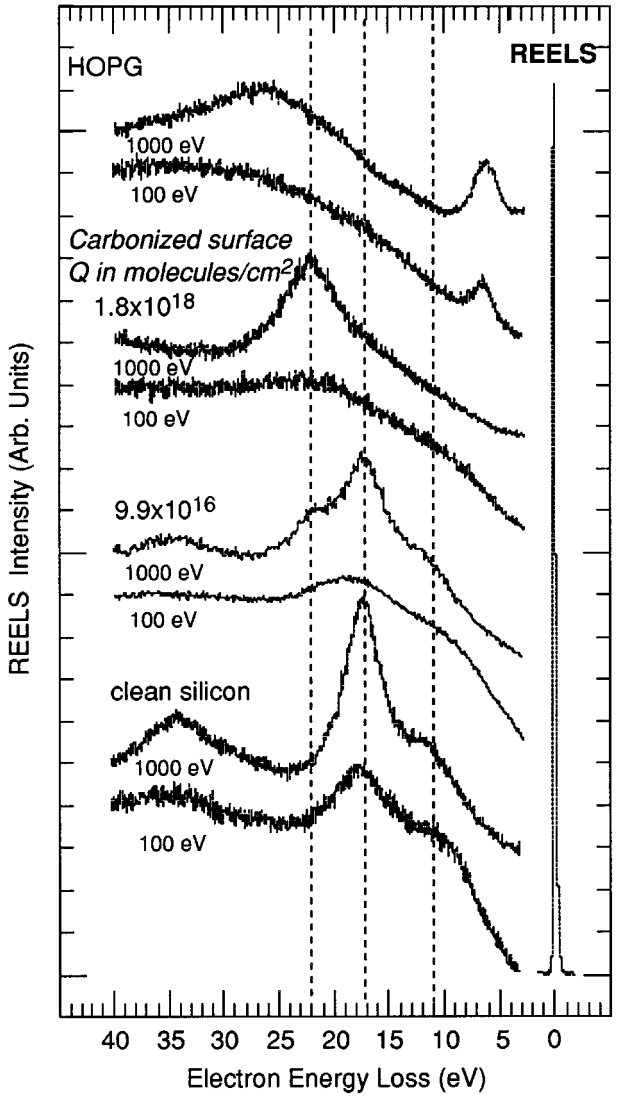

FIG. 8. REELS spectra, taken at $E_p = 100$ eV (surface sensitive) and $E_p = 1000$ eV (bulk sensitive), for the clean Si surface, the carbonized surface at two exposures, and a clean HOPG surface. SiC bulk-plasmon, Si bulk- and Si surface-plasmon losses are at 22, 17, and 11 eV, respectively.

energy difference $\Delta_2 = \mathrm{Si}\ 2p_{3/2}(\mathrm{Si_C}) - \mathrm{C}\ 1s(\mathrm{C_{Si}})$ will be much more suggestive of real variations in the chemical bonding. Indeed Δ_2 is independent of any energy reference (changes in Fermi-level position, charging effects, etc). The variations of Δ_2, $\Delta(\Delta_2)$, can be written as

$$+\Delta V(\mathrm{Si_C}) - \Delta V(\mathrm{C_{Si}}) + \Delta R(\mathrm{Si_C}) - \Delta R(\mathrm{C_{Si}}),$$

where ΔV and ΔR are the variations, respectively, in the initial state (e.g., changes in the nature of the ligands around a given atom) and in the final state (changes in the extra-atomic relaxation energy). As it seems natural to presume that C $1s$ and Si $2p$ holes experience the same extra-atomic relaxation in the carbonized layer, $\Delta(\Delta_2)$ is approximated by $+\Delta V(\mathrm{Si_C}) - \Delta V(\mathrm{C_{Si}})$. A measurable variation of Δ_2, $\Delta(\Delta_2) = +0.40 \pm 0.15$ eV, is clearly seen in Fig. 7(b) between the first steps of carbonization and the $Q \sim 10^{18}$ molecules/cm^2 exposures for which Δ_2 stabilizes at -182.3 ± 0.06 eV. For the 880 °C film Δ_2 is equal to -182.27 ± 0.05 eV. Takagaki, Igari, and Kusunoki[25] after carbonization of silicon in ethylene at 850 °C find Δ_2 equal to -182.2 eV. Recently published Si $2p$ and C $1s$ Al $K\alpha$ spectra of a clean $3C$-SiC surface[50] give a value of $\Delta_2 = 100.3 - 282.5 = -182.2$ eV. Consequently, Δ_2 variation may be the hint of a departure from bulk SiC chemical arrangement for $Q \leqslant 10^{17}$ molecule/cm^2.

The composition of the silicon-carbon compound may be evaluated from the measured $\mathrm{C_{Si}}$-to-$\mathrm{Si_C}$ intensity ratio $I_{\mathrm{C_{Si}}}/I_{\mathrm{Si_C}}$ corrected by a suitable sensitivity factor calculated from tabulated values of the C $1s$ and Si $2p$ cross sections and from the analyzer transmissivity. Rather than calculating a theoretical sensitivity factor (the cross sections are calculated data, the transmissivity is not given explicitly by the manufacturer and the escape depth of C $1s$ and Si $2p$ electrons are estimated values) we prefer to determine an experimental sensitivity factor. Here we have considered the ''reference SiC'' layer formed at 880 °C: the C $1s(\mathrm{C_{Si}})$ to Si $2p_{3/2}(\mathrm{Si_C})$ intensity ratio as a function of the polar angle θ (between 0° and 70°) oscillates by $\pm 5\%$ around an average value $r = 1.31$ essentially because of photoelectron diffraction effects (see below). Dividing the experimental $\mathrm{C_S}$-to-$\mathrm{Si_C}$ intensity ratio by the r factor, we plot $x = (I_{\mathrm{C_{Si}}}/I_{\mathrm{Si_C}}) \times r^{-1}$

versus the exposure Q [Fig. 7(c)]. Obviously this comes down to plotting, an equivalent stoichiometry SiC_x with x equal to one for the 880 °C grown film. We notice that for low Q ($\leqslant 10^{17}$ molecules/cm^2), x values cluster around 0.6, while for large Q ($Q \geqslant 2\times10^{18}$ molecules/cm^2) an equivalent stoichiometry of 1 is reached. This parallels the changes of the Δ_2 parameter with Q [Fig. 7(b)]. If we assume that in the substoichiometric layer, C remains bonded to four silicon atoms and that the C 1s initial state is not modified by changes in atomic coordination beyond the sphere of the first neighbors, then $\Delta(\Delta_2)$ further reduces to $\Delta V(\mathrm{Si_C})$. The increase of $\Delta(\Delta_2)$ suggests that Si bonds to an increasing number of more electronegative C atoms [in Pauling's electronegativity scale $\chi_{Si}=1.8$ and $\chi_C=2.5$ (Ref. 51)]. Consequently, at 820 °C an initial phase of C dissolution into the silicon substrate is likely to precede the formation of the stoichiometric SiC film. Although a detailed analysis of the XPS spectra is indicative of the presence of a substoichiometric ''Si-C alloy,'' the REELS spectra seem not to confirm such evidence. In Fig. 8, for the shortest exposure ($Q=9.9\times10^{16}$ molecules/cm^2), we find, working in bulk sensitive conditions ($E_p=1000$ eV), three peaks at 22, 17, and 11 eV, that are the fingerprints of bulk SiC plasmons,[47] bulk Si plasmons and surface Si plasmons,[52] respectively. Reducing the primary energy to $E_p=100$ eV, in order to work with a greater surface sensitivity, we still observe the Si surface plasmon at 11 eV and a second broad structure at $\sim$20 eV between SiC and Si bulk plasmons. The $\sim$20 eV structure was attributed by Bozso and co-workers[23] to a Si-C alloy that forms at 650 °C and that separates into Si and stoichiometric SiC by annealing at 830 °C. In the present case, the appearance of a broad structure at $\sim$20 eV is trivially due to the merging of the 17 eV (bulk Si) and 22 eV (bulk SiC) plasmon losses, because the Si peak intensity decreases with respect to that of the SiC peak with decreasing E_p, as the Si-C compound is formed at the sample surface. Our interpretation could also apply to the spectra given in Ref. 23, which are indeed very similar to ours. However their poorer energy resolution may have rendered their analysis more delicate (the elastic peak FWHM was about 3 eV instead of 0.46 eV in this work).

Another puzzling point is the observation of a strong increase in Δ_1 [by 0.4 ± 0.1 eV, see Figs. 6 and 7(a)] from $Q=1.2\times10^{17}$ molecules/cm^2 (mean ^{12}C content of 20×10^{15} atoms/cm^2 or an equivalent thickness of $\sim$40 Å) to $Q=1.4\times10^{18}$ molecules/cm^2 (mean ^{12}C content of 122×10^{15} atoms/cm^2), while the equivalent stoichiometry in both cases is close to 1 [Fig. 7(c)] and Δ_2 values coincide within the experimental error. Under the assumption of a negligible band bending over the region probed by photoemission [the escape depth of C 1s and Si 2p photoelectrons is in the range of 20–30 Å (Refs. 23 and 40)], Δ_1 and the valence-band offset (VBO) between the valence-band maxima (VBM) of the SiC film and of the silicon substrate are directly related by the relationship[53]

$$\Delta_1 - [E_{CL}^{\mathrm{VBM}}(\mathrm{SiC}) - E_{CL}^{\mathrm{VBM}}(\mathrm{Si})],$$

where $E_{CL}^{\mathrm{VBM}}(\mathrm{SiC})$ and $E_{CL}^{\mathrm{VBM}}(\mathrm{Si})$ are the Si $2p_{3/2}-$VBM energy separation for SiC and Si, respectively. $[E_{CL}^{\mathrm{VBM}}(\mathrm{SiC})\text{-}E_{CL}^{\mathrm{VBM}}(\mathrm{Si})]$ is a constant, and can be measured from the corresponding Si $2p_{3/2}$ core levels (Fig. 6) and from the VBM's (the valence-band spectra are not shown), for the reference 880 °C grown SiC film and for the clean Si surface, respectively: we find it equal to 0.53 ± 0.20 eV. If the previous assumption were correct, the $\sim$0.4 eV change in Δ_1 should be entirely due to an equivalent increase of the valence-band offset. It is however, much more reasonable to admit that the ''unbent-band'' assumption is not valid when hundreds-of-Å-thick carbide hills [Fig. 3(c)] develop and that a strong band bending downward, or even a charging effect, are present in the SiC probed layers. Thus, VBO can be estimated only for the thin layer ($Q=1.2\times10^{17}$ molecules/cm^2), and amounts to 0.37 ± 0.25 eV. This value can be compared to Robertson's tight-binding calculations[54] (0.85 eV in the pinned limit) and to VBO measurements of a-Si/a-$Si_{1-x}C_x$:H and a-Si/a-$Si_{1-x}C_x$ interfaces given by Fang and Ley[55] (for $x=0.5$, VBO of 0.8 ± 0.1 eV and 0.40 ± 0.1 eV for the hydrogenated and dehydrogenated material, respectively).

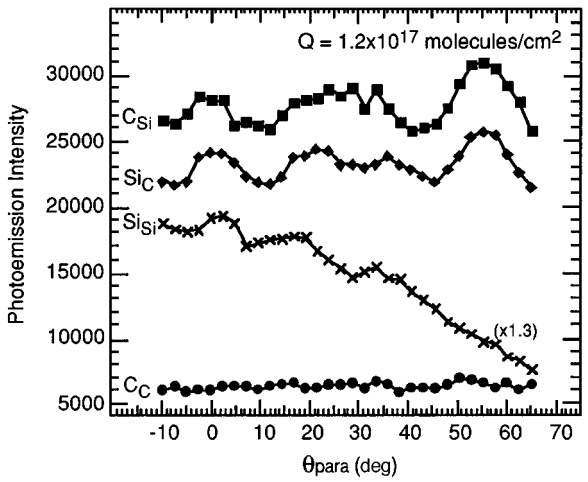

FIG. 9. Polar angle variation (in ''para'' geometry) of the Si_{Si} and Si_C components of the Si $2p_{3/2}$ line on the one hand, and of the C_C and C_{Si} components of the C 1s line on the other hand, for a silicon surface exposed to a dose of 1.2×10^{17} molecules/cm^{-2} at 820 °C.

D. Short-range order as probed by XPD

1. Experimental XPD patterns

As stated before, the Si 2p and C 1s core levels can be decomposed into two chemically shifted components Si_{Si} and Si_C on the one hand, and C_C and C_{Si} on the other hand. Changes in their intensities as the photoelectron emission angle increases will be informative, first of their relative in-depth distribution, second on the degree of orientational order through intensity modulations arising from photoelectron diffraction effects. Indeed in the photoelectron kinetic energy of interest ($\sim$1153 eV for Si 2p and 970 eV for C 1s) the dominant effect is the forward focusing, and the prominent peaks are expected at angles corresponding to atomic row directions.[56] A representative case is given in Fig. 9, where the angular behavior of the various chemical states of Si $2p_{3/2}$ and C 1s are plotted for an exposure Q of 1.2×10^{17} molecules/cm^2, i.e., for a thin film of equivalent thickness about 40 Å. While the intensities of Si_{Si}, Si_C, C_{Si}

all exhibit modulations due to photoelectron diffraction effects, that of C_C is featureless. Moreover, the Si_{Si} intensity decreases with respect to that of Si_C as the polar angle θ increases: this behavior clearly indicates that the elemental silicon is buried under the growing carbide and does not ''float'' as often reported in this range of carbonization temperature.[23,33] On the other hand, the C_C line intensity does not vary much with θ: this can be assigned to a discontinuous overlayer, e.g., carbon particles at the surface. At higher exposures, the C_C relative intensity increases with increasing values of θ, indicative of its presence in the top layers.

We report in Fig. 10 the angle-dependent modulations of the clean substrate Si_{Si} component and those of the carbonized surface Si_C component, when the intensity of the latter has been extracted by the fitting procedure. This is done for $Q \geqslant 1.2\times10^{17}$ molecules/cm^2, when Si_C weight is clearly sufficient. The Si_C polar curves, whatever the exposure and the azimuth plane (''ortho'' versus ''para'') present similar diffraction structures. All of them exhibit peaks at angles θ corresponding to the crystallographic directions [001], [114]/[114], [112]/[112], [111]/[111] of the silicon substrate. This means that a conspicuous fraction of the carbon-bonded silicon atoms pertains to atomic rows aligned with major directions of the underlying silicon substrate even in cases where a long-range probe like RHEED indicates a disordered polycrystalline growth. One important parameter is the contrast $f_{[hkl]}$ of a given diffraction peak referred to a substrate direction $[hkl]$, and defined as $(I_{max}-I_{min})/I_{max}$, where I_{max} is the intensity maximum and I_{min} that of the corresponding first minimum. Our data show that $f_{\langle 111\rangle}$ in particular is larger for $Q=1.2\times10^{17}$ molecules/cm^2 (20×10^{15} ^{12}C atoms/cm^2) than for the subsequent exposures.

In contrast with the Si $2p(Si_C)$ signal, which at very low coverage is obscured by the substrate contribution, the largely dominant C $1s(C_{Si})$ component allows us to observe the appearance of angle-dependent modulations from the very beginning of growth (Fig. 11). One can observe two ''peaked'' structures in directions aligned with [001] and [111]/[111] substrate directions, and a broad structure in between. Again, the general trend is that the contrast $f_{\langle 111\rangle}$ diminishes (by a factor of ~3) with increasing thicknesses. For small acetylene doses ($Q<10^{17}$ molecules/cm^2), the dominant diffraction peak is in the $\langle 111\rangle$ substrate direction. This indicates that in the initial carbonization step also, carbon is likely to be surrounded by silicon scatterers in $\langle 111\rangle$ substrate directions, that is, C is sp^3 bonded to silicon, without measurable tetragonal distortion.

Diani and co-workers[33,36] have recently published experimental XPD data on carbonized Si(001) and on $3C$-SiC. Their analysis conditions are equivalent to ours, in particular the XPD curves of the clean Si(001) surface in the {110} azimuth plane (Fig. 5 of Ref. 33 and Fig. 3 of Ref. 36) are very similar to the curve we report in Fig. 10 (we have found the same contrast in the [001] direction). Thus, we report in Table II the contrast factors f obtained for polar scans in {110} azimuth planes for a film grown at 850 °C with activated CH_4,[33] of estimated thickness ~37 Å (by XPS), and for a state-of-the-art $3C$-SiC *single-crystal* film of thickness 5.7 μm.[36] The contrasts we find (especially for small Q) are close to the ones given for the thin-film grown in activated

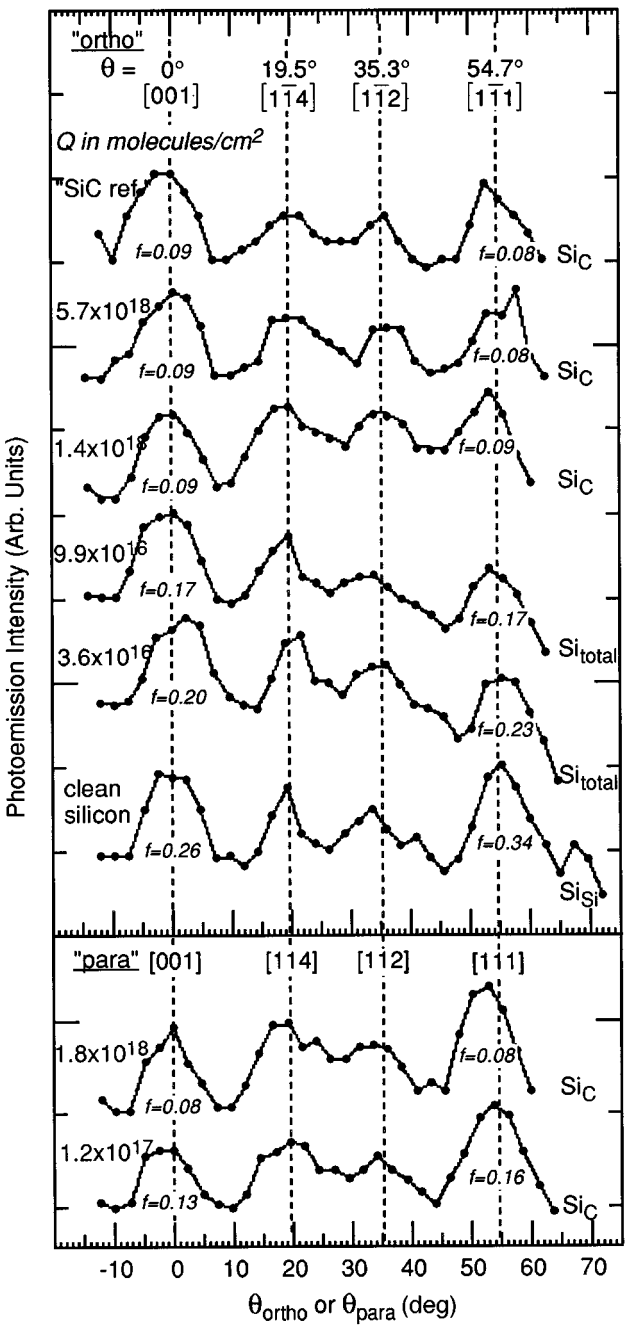

FIG. 10. Polar angle variations of the Si $2p_{3/2}$ components (Si_{Si}, Si_{total}, Si_C) for increasing exposures Q expressed in molecules/cm^2. Scans in the ''ortho'' and ''para'' geometry are given, that is, in the Si(110) azimuthal plane and close to the Si (110) azimuthal plane, respectively. The XPD curves of the clean surface and of the ''SiC reference'' (the 880 °C-grown film) are also given.

methane, but they remain much smaller than the ones obtained for the SiC crystal (up to a factor of 4 smaller for the large Q films). Consequently, experimental contrasts that depart from those of the single crystal give a clear indication of a SiC growth not well registered with respect to the substrate.

Even for films indicated as polycrystalline by RHEED, we continue to observe diffraction peaks precisely in the directions expected when forward scattering dominates, under the assumption that the ''cube-on-cube'' heteroepitaxial re-

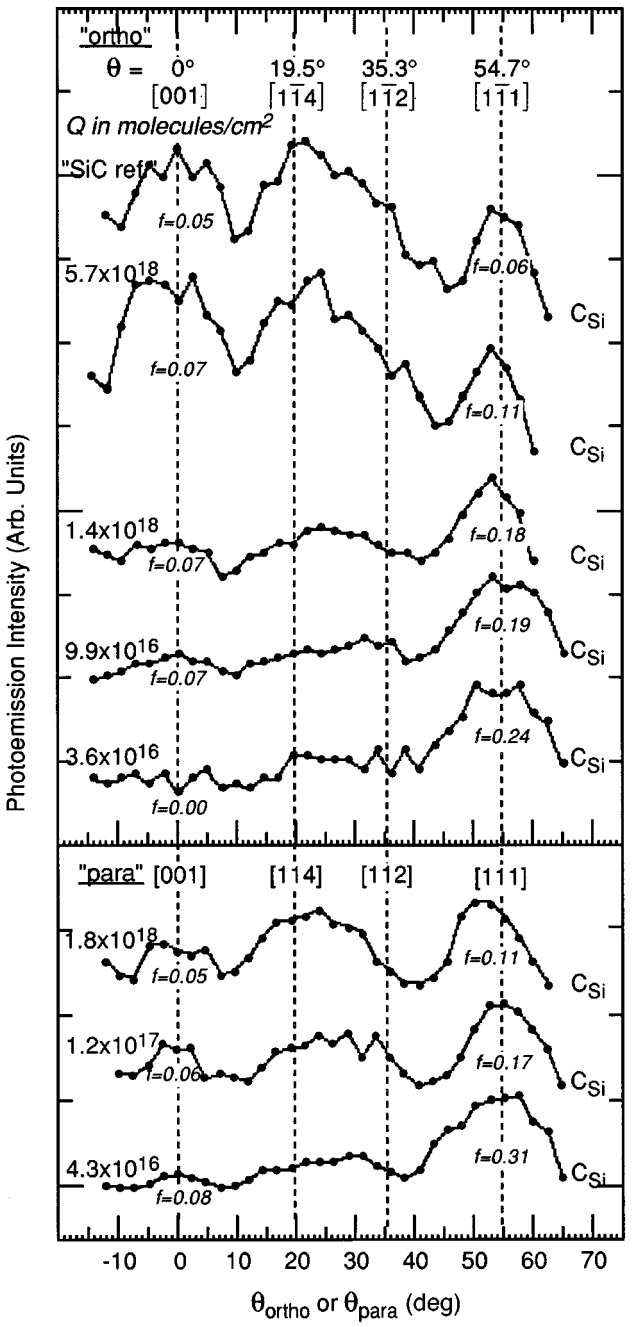

FIG. 11. Polar angle variations of the C_{Si} component of C 1*s* for increasing exposures *Q* expressed in molecules/cm^2. Scans in the ''ortho'' and ''para'' geometry are given, that is, in the Si(110) Si azimuthal plane and close to the Si(110) azimuthal plane, respectively. The XPD curves of the clean surface and of the ''SiC reference'' (the 880 °C-grown film) are also given.

lation is fulfilled. It is clear that if all crystallites were randomly oriented with respect to the substrate, featureless experimental XPD curves ($f=0$) would result. So we can hypothesize that a substantial fraction of the probed material remains aligned with respect to the substrate, the remaining part being randomly oriented. On the basis of these results we conclude that the polycrystalline ring-shaped RHEED patterns are essentially produced by the volcanoes. The structured XPD signal may originate from the flat areas in between the volcanoes, covered with a SiC layer which remains very thin (a few tens of Å, the substrate Si_{Si} component being still detected at $\theta=0°$) and ordered with respect to the substrate.

Let us now come back to one of the major interrogations of our study: Does the initial array of asymmetrically shaped terraces and bisteps act as a template for the oriented growth of SiC? Indeed a peculiarity of the ZnS structure is that the (110) and (110) planes are not equivalent (see Fig. 12). If one SiC plane, (110) or (110), is preferentially aligned with the (110) substrate plane, different XPD patterns are expected in the ''ortho'' and ''para'' geometries, for Si $2p(Si_C)$ and especially for C $1s(C_{Si})$, as the XPD pattern simulations, given below, will show it. A comparison with already published experimental data from ''single'' crystals is certainly useful. Nevertheless, there is always some uncertainty concerning the degree of elimination of APB's, even in the best commercial films (see Ref. 32). Thus a comparison with calculated XPD patterns of 3*C*-SiC in well chosen azimuths is necessary. That is why we have calculated the polar diffraction patterns of a 3*C*-SiC(001) crystal in the (110) and $(\bar{1}10)$ planes [denoted in the following SiC(110) and SiC(110)], considering that the ''cube-on-cube'' heteroepitaxial relationship of 3*C*-SiC on Si is the most likely, as indicated by RHEED.

2. Theoretical XPD patterns

A refined analysis of experimental data requires the consideration of several problems relative to the calculation of XPD patterns.[57] Namely, (i) cluster convergence, (ii) the use of a realistic value of the mean-free path, and (iii) effects induced by multiple scattering. Theoretical problems are constituted by the convergence in the number of atoms needed to reproduce the observed photoemission intensity. In the past, substantial discrepancy has been found in the comparison of the experimental data with a single-scattering theory for clusters whose dimensions were comparable with the estimated value of electron mean-free-path in the solid, even for the high kinetic-energy regime. This is probably due to a greater complexity of the process underlying the loss of coherence of the primary photoelectron wave. A more realistic picture could be achieved by introducing defocussing effects, first discussed by Poon and Tong,[58] which affects diffraction along rows of atoms in the crystal. The introduction of additional scattering events proved to be crucial in obtaining cluster convergence at ''physical'' sizes and good comparison with the experiment. Very recently, a similar breakdown of single-scattering analysis has been evidenced by Chen *et al.*[59]

The whole calculations presented here are based on a scattering matrix method derived by that of Rehr and Albers[60] and recently applied in Ref. 61. This method replaces the plane-wave scattering factor by scattering matrices that account for the spherical character of the incoming and outgoing photoelectrons waves. We set the dimension of this matrix up to 6, which, as we checked by increasing this value, leads to results almost indistinguishable from the full spherical wave calculation. Due to the pronounced peaking of the scattering factor in the forward direction, we may neglect all the multiple scattering pathways with scattering angle larger than 30°. Complex phase shifts have been calculated up to a maximum value of the angular momentum (l_{max}) equal to 23 by means of a Hedin-Lundqvist potential

TABLE II. Contrast $f^{X}_{[hkl]}$ for a given chemical component X, referred to $[hkl]$ directions of the substrate for carbonized Si(001) surfaces or those of the SiC(001) single crystal. ''Eq. thick.'' stands for ''equivalent thickness.''

Experimental contrast	$f^{Si_C}_{[001]}$	$f^{Si_C}_{\langle 111\rangle}$	$f^{C_{Si}}_{[001]}$	$f^{C_{Si}}_{\langle 111\rangle}$
SiC crystal[a]	43% (1$\underline{1}$0)	~36% (1$\underline{1}$0)	~30% (1$\underline{1}$0)	~35% (1$\underline{1}$0)
	45% (110)	~36% (110)	~34% (110)	~40% (110)
Activated CH_4/Si[b]	~14%	~16%	~8%	~20%
C_2H_2/Si[c]				
Eq. thick.≤40 Å	~13%	~16%	~7%	31–17%
Eq. thick.>200 Å	~9%	~10%	~7%	~10%

[a]From Ref. 36.
[b]From Ref. 33.
[c]This work.

as recently applied to x-ray absorption study.[62] In some particular scattering conditions, the calculated electron mean-free path, which is almost isotropic in its definition can fail in reproducing the strong anisotropies observed in some cases both in scattering and damping of the electronic waves.

A surface slab containing six double Si/C (or C/Si) planes is considered in the calculations which are performed both in the single-scattering approach (SS) and in the multiple-scattering (MS) approach. To our knowledge, only SS calculations of $3C$-SiC XPD patterns have been published[36] until now. Such a cluster size corresponds to a mean-free path in the solid of the order 15–20 Å traveled by electrons having kinetic energy of 1100–1400 eV and a number of atoms of the order of 500–700. The theoretical XPD curves of Si $2p$ for polar scans in the SiC(110) and SiC planes are reported in Fig. 13. The corresponding C $1s$ simulated patterns are reported in Figs. 14 and 15.

With respect to the SS calculations, the main effect of the MS approach is to reduce the peak intensity along main crystal directions, especially in the case of C $1s$ photoemission. The strong element dependence of the photoelectron diffraction in SiC, previously evidenced theoretically and experimentally by Juillaguet *et al.*,[36] is the reason for the different behavior of Si and C with respect to the number of scattering events used in the approximation. While the Si atoms are only slightly perturbed by the C atoms, with the net result of a photoelectron diffraction Si $2p$ pattern almost completely due to the Si atoms fcc sublattice (Fig. 12), the carbon atoms receive a great influence from Si atoms lying close to the scattering planes but having greater scattering power. The consequence of this picture is that while Si atoms are far enough to feel a reduced influence from the MS, the carbon feels strong effects from collinear Si atoms. The MS calculations have been done up to the third order of scattering (suitable for the range of kinetic energy used, as put in evidence from Kaduwela, Friedmann, and Fadley[63]) with an acceptance cone of scattering, i.e., the half-opening angle of the cone around the forward-scattering direction inside which a scattering event has a nontrivial probability to occur, of 30°.

The greater scattering power of silicon atoms with respect to that of carbon atoms means that the calculated C $1s$ patterns are also very sensitive to the surface termination of the SiC crystal, i.e., C-terminated or Si-terminated. Interferences

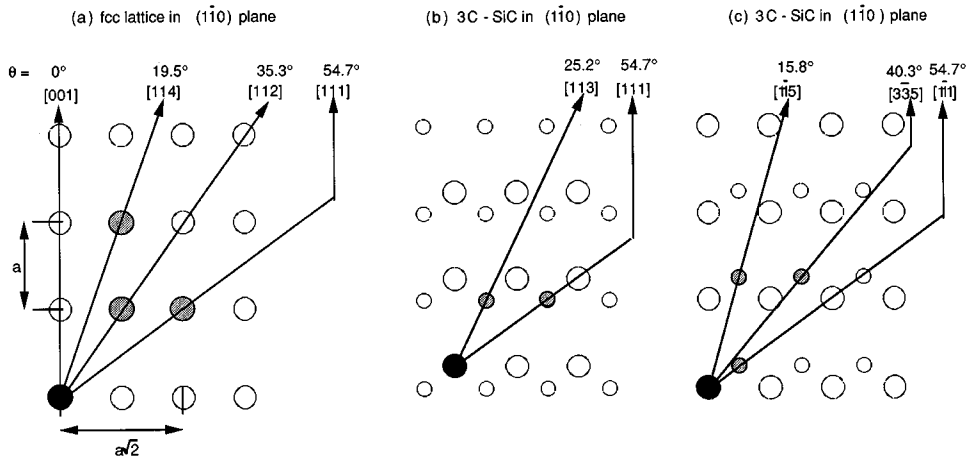

FIG. 12. Side views of the atomic structures for (a) $(1\bar{1}0)$ plane of the fcc lattice accounting for the Si or C sublattices in 3C-SiC. (b) (110) plane for the zinc-blende SiC structure. (c) (110) plane for the zinc-blende SiC structure. Small and large circles represent Si and C atoms, respectively. Black and gray circles represent emitters and scatterers, respectively. Note that (110) and (110) planes are equivalent in the fcc structure but not in the ZnS one.

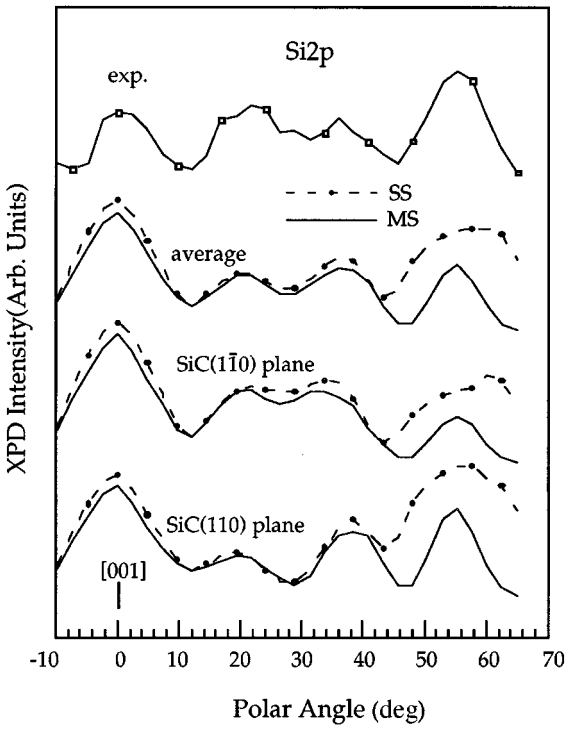

FIG. 13. Calculated XPD patterns of Si $2p$ in the SiC(110) plane, in the SiC(110) and averaged on both planes. (SS, single scattering; MS, multiple scattering.) An experimental Si $2p(\mathrm{Si_C})$ XPD pattern in ''para'' geometry is given for comparison ($Q = 1.2\times10^{17}$ molecules/cm^2).

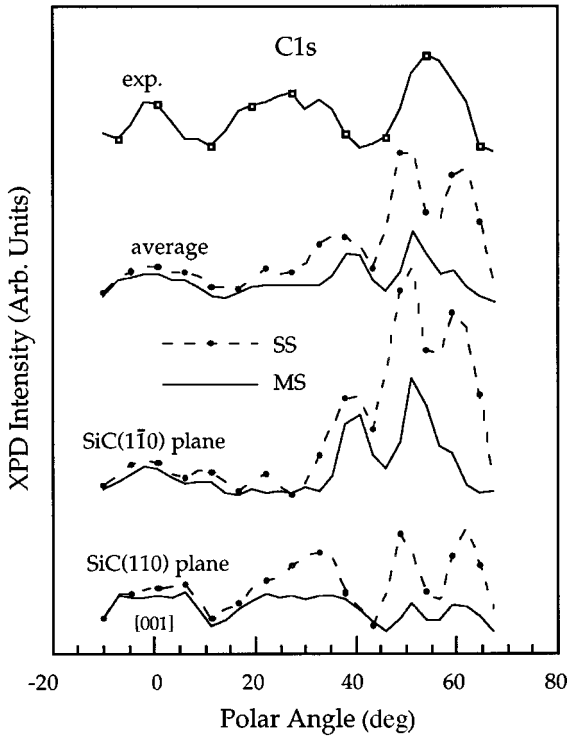

FIG. 15. Calculated XPD patterns of C $1s$ in the SiC(110) plane (average of the two patterns of Fig. 14), in the SiC(110) and averaged on both planes (SS, single scattering; MS, multiple scattering). An experimental C $1s(\mathrm{C_{Si}})$ XPD pattern in ''para'' geometry is given for comparison ($Q = 1.2\times10^{17}$ molecules/cm^2).

induced by Si scatterers in the C fcc sublattice, in particular for scattering along the [117] direction of the SiC(110) plane modify the shape of the diffraction peak in the [001] direction. This is shown in Fig. 14 where calculated C $1s$ patterns in the SiC(110) plane are reported for the two different terminations of the surface. It is clear that the Si terminated surface, with the last Si atoms as scatterers in the [117] direction, produce a U-shaped [001] diffraction peak. This effect disappears when the surface is terminated by C atoms. The (110) calculated pattern given in Fig. 15 is the average of the two C- and Si-terminated curves. We note, however, that for a reconstructed Si-terminated SiC surface (e.g., with Si dimers) the interference effect, leading to a U-shaped [001] peak, should be strongly reduced. Nevertheless, calculated and experimental C $1s$ XPD patterns of the SiC(110) plane given in Ref. 36 present a U-shaped [001] photodiffraction peak, although the LEED patterns were indicative of 2×1 reconstructed single domain, attributed to a surface termination by Si dimers.

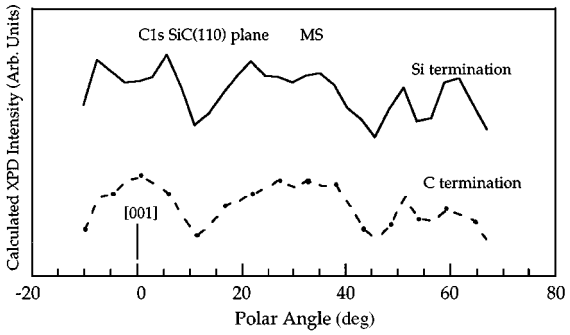

FIG. 14. Effects of Si and C surface termination in the case of a XPD theoretical pattern of C $1s$, in the SiC(110) plane. (MS, multiple scattering)

As XPD patterns calculated in the inequivalent SiC(110) and SiC(110) planes, exhibit sizable differences, both for Si $2p$ and C $1s$, we can in principle determine the orientation of the growing SiC crystallites, in the case of a ''cube-on-cube'' heteroepitaxy, that is the orientation of a given SiC{110} plane with respect to the initial Si bistep direction ([110]). For both SiC{110} planes, the calculated Si $2p$ curves (Fig. 13) exhibit maxima close to angles corresponding to the fcc Si-sublattice atomic rows (i.e., SiC [001], [114]/[114], [112]/[112], and [111]/[111]). However, the SiC(110) and SiC(110) patterns are not identical. In particular in the SiC(110) plane the diffraction peak due to the [111] collinear scattering with the very close C atom (see Fig. 12) has a greater intensity than that of [111] peak in the SiC(110) plane. On the other hand, the low intensity in the calculations along the direction [114] in the SiC(110) polar pattern could be explained in terms of a too strong complex potential, damping the scattering events between the two far Si atoms (9.2 Å) involved. In the case of the SiC(110) polar pattern some contributions to the intensity in the [114] direction are possibly provided by interference with Si-C scattering along [113] direction, which is favored with respect to the [115] scattering happening in the case of the SiC(110) patterns, because of the shorter distance between emitter and scatterer.

In comparison with calculated Si $2p$ patterns, the calculated C $1s$ curves (Fig. 15) exhibit many marked differences according to the considered azimuths: indeed in the

SiC($\bar{1}10$) plane, the [111] peak crushes down the other contributions, while in the SiC(110) plane three structures of equivalent contrast are foreseen. This can be simply explained as follows. In the SiC(110) polar pattern, the [113] peak and those close to this one, [117] and [337], connect the C emitter and Si scatterers at a distance which is much shorter than that relative to [119] and [113] scattering directions in the SiC(110) plane which present a sizable decrease of the scattering intensity. Once more, the strong reduction of intensity at $\sim 54°$, in the [111] direction in the SiC(110) plane, corresponding to a long-distance scattering (6.6 Å), should be due to a too strong complex potential along this direction, inherent with the quasi-isotropic modelization of the loss processes inside the solid. Apart from the relative diffraction peak intensities, the main features of the present C 1*s* patterns, calculated with the MS approach, are similar to the calculated curves of Ref. 36. However, strong discrepancies with the experimental C 1*s* XPD pattern[36] can be noticed, especially in the SiC(110) plane, for which the [001] and [111] diffraction peaks have similar contrast factors (Table II). This may be due to the fact that the SiC film used in Ref. 36 is not entirely a single crystal.

Let us now examine if our calculated XPD patterns can give evidences for a ''biased'' SiC growth due to a preferential shrinkage of the [110] Si row (perpendicularly to the initial bistep edges), as proposed by Kitabatake and Greene.[31] In such a case, 3*C*-SiC should form with Si-C-Si bonding directions along the substrate [110] direction (see Fig. 2). This means that SiC(110) XPD patterns should be obtained for ''ortho'' scans and SiC(110) XPD patterns for ''para'' scans (see Figs. 2 and 12). First we consider the experimental Si $2p(\mathrm{Si_C})$ pattern obtained in ''para'' geometry for the ~ 40 Å thick ''heteroepitaxied'' SiC film ($Q = 1.2\times 10^{17}$ molecules/cm^2), given in Fig. 10, and reported in Fig. 13 to ease comparison. It is impossible from the relative peak intensities in the $\langle 114\rangle$ and $\langle 111\rangle$ directions to choose any of the two possible growth orientation. Instead, the theoretical curve averaged on the two SiC{110} planes bears a closer resemblance to the experimental $\mathrm{Si_C}$ polar scan.

The experimental C $1s(\mathrm{C_{Si}})$ patterns should be more informative. If the asymmetric shrinkage is acting perpendicularly to the step edges, then a dominating [111] diffraction peak must be observed in ''para'' geometry and three structures of equivalent intensity in ''ortho'' geometry. For the small acetylene doses Q (till 9.9×10^{16} molecules/cm^2), no appreciable differences between the experimental XPD curves (Fig. 11) are observed, as a strong $\langle 111\rangle$ diffraction peak is seen both in the ''ortho'' and ''para'' geometries. It can been argued that, in this case, the stoichiometric compound is not yet produced and that a comparison with 3*C*-SiC calculated data is not entirely relevant. On the other hand, the XPD pattern of the ~ 40 Å thick ''heteroepitaxied'' SiC film ($Q = 1.2\times 10^{17}$ molecules/cm^2) measured in ''para'' geometry can offer a good test for the asymmetric shrinkage model. As the [111] diffraction does not dominate over the other diffraction peaks (Figs. 11 and 15), there is no hint of a preferential shrinkage in a direction perpendicular to the initial bistep edges.

In conclusion, the comparison of theoretical and experimental XPD patterns does not give evidence, in the present experimental conditions, of a ''biased'' shrinkage mechanism in a direction perpendicular to the initial silicon bistep edges, as proposed in Ref. 31. Apparently neither the asymmetry in the terrace shape nor the presence of a 2×1 reconstructed *single* domain can allow silicon carbide to grow with a preferential orientation of one of the two inequivalent SiC{110} planes with respect to Si(110).

E. Growth mechanisms

Both on experimental and theoretical grounds, Kitabatake and co-workers in their more recent paper[31] consider that the ''[110] shrinking row'' mechanism, described in the introductory part of this paper, is the main process leading to SiC growth. If such a mechanism is the only one to exist, an abrupt Si/SiC interface must result. This is in sharp contrast with the evidence we have of an initial carbonization step, where C atoms diffuse from the surface into the silicon lattice, to find sites characterized by a clear chemical order. Indeed, XPS C 1*s* binding-energy position gives evidence for C atoms bonding to Si atoms, and XPD curves show that these carbon emitters have scatterers in the $\langle 111\rangle$ directions of the silicon substrate, although a strong distortion of the Si lattice around an isolated C atom is expected, due to the large bond-length difference between Si-C and Si-Si. This important issue has been addressed recently by Rücker *et al.*,[64] both theoretically and experimentally. These authors have reported on strained stabilized $\mathrm{Si_{1-y}C_y}$ (with y up to 20%) layers on Si, grown by MBE at 600 °C and devoid of SiC precipitation. Their calculations (based on density-functional theory and a Keating model) predict that embedded layers with stoichiometry $\mathrm{Si_{n-1}C}$ (with $n \geqslant 4$) are considerably more stable than isolated C impurities. In their model, nearest-neighbor C-C pairs are excluded, because of the too short C-C bond length. Rather, C atoms tend to arrange as third-nearest neighbors (for $n \geqslant 5$), in a sixfold ring where two opposite Si are replaced by two C atoms. Then the bond lengths relax while maintaining the ideal tetrahedral bond angles. This could explain why we still observe intense diffraction peaks for the $\mathrm{C_{Si}}$ component in the $\langle 111\rangle$ directions. We believe that such configurations can explain the departure from stoichiometry we infer from both the $\mathrm{Si_C}$ to $\mathrm{C_{Si}}$ ratio and the change in the binding-energy difference Δ_2. We note that the molecular simulations (published in the paper of Kitabatake, Deguchi, and Hirao[26]) did not exclude that, in some circumstances, C atoms can penetrate in the silicon subsurface. Let us mention that Auger spectroscopy and thermally programmed desorption, used in combination to study the thermal stability of a layer of $\mathrm{C_2H_2}$ chemisorbed on Si(001), allowed Yates and co-workers to show that the carbon atoms penetrate into the silicon bulk immediately after the beginning of $\mathrm{H_2}$ desorption.[5]

The loss of the regular array of bisteps can have a manifold origin. It can be due to the formation of terraces and steps having, respectively, a large distribution of widths and heights. Silicon step edges can move because of Si surface diffusion and consumption by the carbonization process (or because of etching by atomic hydrogen released by the decomposition of the molecule, see Ref. 24) and coalesce when

they reach pinning centers (SiC nuclei, for example). As faceting is observed in the four ⟨110⟩ azimuths, this means that there is no preferential reorganization (bunching) of [110] oriented steps, as one would expect, given the initial misorientation. This suggests that steps, oriented along [110], are also formed. Provided that shrinking is not biased in a particular ⟨110⟩ direction (see the introductory section and Fig. 1), the ''shrinking row model'' gives a simple explanation for the production of steps both along [110] and [110] (monosteps are formed).

Actually, there is no definite incompatibility between both envisioned scenarios. In order to allow the growth a SiC crystal, the ⟨110⟩ row shrinkage mechanism needs to be accompanied by silicon transport onto the growth surface: we note that in the first version of their model, Kitabatake, Deguchi, and Hirao[26] suggested that surface diffusing Si atoms could precisely originate from those silicon substrate zones disordered by the diffusion path of C atoms. Thus, in the present experimental conditions, the only *caveat* we see against Kitabatake's ''shrinking row'' mechanism are the following: first, it cannot be the only mechanism which is operative (since C in-diffusion has been evidenced). Second, the very narrow width of the initial terraces (~ 31 Å) does not imply necessarily that the shrinkage mechanism occurs only in the direction perpendicular to the initial step edges. Moreover, for a vicinal surface with bisteps, the dangling bonds of the top layer silicons are contained in a plane parallel to the bistep edge direction. Consequently, if carbon atoms are deposited on the surface, Si—C—Si bonds should form, oriented in a direction parallel to the bistep edges, and shrinking should also occur in that direction. The situation changes if C atoms replace Si atoms of the top layer, through a place-exchange mechanism. Then shrinking occurs in a direction perpendicular to the bistep edge. However, this possibility has not been envisaged by Kitabatake and coworkers.

At the very beginning of the carbonization process, the LEED patterns do not exhibit the Si(001)-$c4\times4$ reconstruction observed by Takaoka, Takagaki, and Kusunoki[24] after an exposure of a Si(001)-2×1 surface to ethylene at a temperature around 600 °C, leading to a carbon coverage of about one fourth of a monolayer. Indeed, only a Si(001) 1×1 reconstruction is seen. Moreover, when the SiC layer grows we do not observe any of the Si-rich or C-rich $3C$-SiC(001) reconstruction observed by Kaplan.[47] We attribute this general absence of characteristic LEED patterns, all along the carbonization process, to the presence of C adatoms in excess on the growth surface, forming a disordered carbon layer.

In almost all existing processes, the term ''buffer layer'' is generally used for the first layer grown by direct carbonization. The term ''barrier layer'' should be more appropriate as ''buffer layer'' evokes a compositional graded interface, accommodating the lattice mismatch between Si and SiC. Indeed the essential role of the ''barrier layer'' is to block the out diffusion of silicon atoms from the substrate during the high-temperature CVD processes (at ~ 1300 °C) and the correlative formation of voids. The volcano growth regime that supersedes the initial growth regime, during which a film of ~ 40 Å grows, points to the crucial role played by open channels—left by an incomplete coalescence of SiC nuclei—*even at a temperature as low as 820 °C*. Indeed hillock formation has already been observed and described by Li and Steckl,[18] but for carbidization of silicon at 1300 °C in propane. Cross-sectional SEM observations shown in Ref. 18 prove the existence of unsealed channels at the center of the hillocks, that permit the out migration of Si atoms (the image of a volcano is then rather sound). Indeed, it is expected that the SiC crystal is a diffusion barrier to Si (and C) and that Si migration should occur along easy paths. If we follow the conclusions of Li and Steckl on the carbonization of silicon in C_3H_8 ambient, the use of a higher acetylene pressure should increase the density SiC nucleation centers and in turn favor the coalescence of a continuous hole-free thin SiC layer.

IV. CONCLUSION

The aim of the present work was to investigate, by a combination of *in situ* and *ex situ* characterization techniques, the chemistry, order, morphology, and growth mechanisms of films formed by reaction of a vicinal Si surface (Si(001)-5°[110]) with acetylene at 820 °C.

This ''moderate'' temperature, compatible with silicon technological processing, allowed us to observe a variety of growth processes. During the very initial step of carbonization we have evidenced, by examination of the XPS core-level shifts and of the XPD curves, that a mechanism of carbon dissolution into the silicon substrate acts in parallel with the formation of heteroepitaxial (unstrained) $3C$-SiC nuclei observed by RHEED (twinning is also active). A direct consequence of the atomic transport leading to carbide formation is the destruction of the original array of bisteps and singly oriented terraces of the vicinal silicon surface, and its facetting (LEED). For their part, C 1*s* and Si 2*p* XPD curves, obtained from a ~ 40 Å film, are also characteristic of an oriented growth, but a comparison with calculated curves does not indicate a preferential orientation of any of the two nonequivalent $3C$-SiC{110} planes with respect to the initial bistep edge direction. Thus off-axis silicon surfaces, exhibiting a single Si bond orientation in the outermost plane, cannot act systematically as templates for carbide growth—with obvious negative consequences on the elimination of antiphase boundary domains. We conclude that the ''asymmetric [110] row shrinkage'' model, proposed very recently by Kitabatake and Greene,[31] cannot be applied with all the strength of generality to the carbonization of vicinal surfaces. The role of easy paths for bulk Si out migration through a crystalline carbide quasicontinuous thin film, has also been evidenced at a temperature as low as 820 °C, as polycrystalline carbide grows, precisely where Si atoms emerge.

As a comparison with previous works shows that we lack a unified picture explaining how SiC nucleates on the silicon surface, mass transport phenomena on the surface, and nucleation processes during carbonization with hydrocarbons deserve an extensive study. These are directions for a future work.

ACKNOWLEDGMENTS

We thank Dr. D. Sébilleau (University of Rennes, France) for providing us with the multiple-scattering photoelectron diffraction code. This work was supported in part by the French-Italian Programme d'Actions Intégrées Galilée No. 96007 (Ministère Français des Affaires Étrangères) and by Centre National de la Recherche Scientifique (France) under GDR86.

*FAX: +33 1 44 27 62 26. Electronic address: roch@ccr.jussieu.fr

[1] J. Yoshinobu, H. Tsuda, M. Onchi, and M. Nishijima, Chem. Phys. Lett. **130**, 170 (1986).

[2] M. Nishijima, J. Yoshinobu, H. Tsuda, and M. Onchi, Surf. Sci. **192**, 383 (1987).

[3] M. N. Piancastelli, R. Zanoni, D. W. Niles, and G. Margaritondo, Solid State Commun. **72**, 635 (1989).

[4] C. C. Cheng, R. M. Wallace, P. A. Taylor, W. J. Choyke, and J. T. Yates, Jr., J. Appl. Phys. **67**, 3693 (1990).

[5] C. C. Cheng, P. A. Taylor, R. M. Wallace, H. Gutleben, L. Clemen, M. L. Colaianni, P. J. Chen, W. H. Weinberg, W. J. Choyke, and J. T. Yates, Jr., Thin Solid Films **225**, 196 (1993), and references therein.

[6] J. Yoshinobu, D. Fukushi, M. Uda, E. Nomura, and M. Aono, Phys. Rev. B **46**, 9520 (1992).

[7] C. Huang, W. Widdra, X. S. Wang, and W. H. Weinberg, J. Vac. Sci. Technol. A **11**, 2250 (1993).

[8] M. N. Piancastelli, N. Motta, A. Sgarlata, A. Balzarotti, and M. De Crescenzi, Phys. Rev. B **48**, 17 892 (1993).

[9] Y. Chen, Zh. Liu, Q. Zhang, K. Feng, and Zh. Lin, Appl. Phys. Lett. **67**, 2936 (1995).

[10] B. I. Craig and P. V. Smith, Surf. Sci. **276**, 174 (1992).

[11] R.-H. Zhou, P.-L. Cao, and L.-Q. Lee, Phys. Rev. B **47**, 10 601 (1993).

[12] Q. Liu and R. Hoffmann, J. Am. Chem. Soc. **117**, 4082 (1995).

[13] T. Sugii, T. Ito, Y. Furumura, M. Doki, F. Mieno, and M. Maeda, IEEE Electron Device Lett. **EDL-9**, 87 (1988).

[14] S. Nishino, J. A. Powell, and H. A. Hill, Appl. Phys. Lett. **42**, 460 (1983).

[15] S. Nishino, H. Suhara, H. Ono, and H. Matsunami, J. Appl. Phys. **61**, 4889 (1987).

[16] O. Kordina, L. O. Björketun, A. Henry, C. Hallin, R. C. Glass, L. Hultman, J. E. Sundgren, and E. Janzén, J. Cryst. Growth **154**, 303 (1995).

[17] J. P. Li, A. J. Steckl, I. Golecki, F. Reidinger, L. Wang, X. J. Ning, and P. Pirouz, Appl. Phys. Lett. **62**, 3135 (1993).

[18] J. P. Li and A. J. Steckl, J. Electrochem. Soc. **142**, 634 (1995).

[19] I. H. Khan and R. N. Summergrad, Appl. Phys. Lett. **11**, 12 (1967).

[20] C. J. Mogab and H. J. Leamy, J. Appl. Phys. **45**, 1075 (1974).

[21] I. Kusunoki, M. Hiroi, T. Sato, Y. Igari, and S. Tomoda, Appl. Surf. Sci. **45**, 171 (1990).

[22] I. Kusunoki and Y. Igari, Appl. Surf. Sci. **59**, 95 (1992).

[23] F. Bozso, J. T. Yates, Jr., W. J. Choyke, and L. Muelhoff, J. Appl. Phys. **57**, 2771 (1985).

[24] T. Takaoka, T. Takagaki, and I. Kusunoki, Surf. Sci. **347**, 105 (1996).

[25] T. Takagaki, Y. Igari, and I. Kusunoki, Appl. Surf. Sci. **92**, 287 (1996).

[26] M. Kitabatake, M. Deguchi, and T. Hirao, J. Appl. Phys. **74**, 4438 (1993).

[27] *Physics of Group IV Elements and III-V Compounds*, edited by O. Madekeng, Landolt-Bornstein, New Series, Vol. 17 (Springer-Verlag, Berlin, 1982).

[28] K. Shibra, S. Nishino, and H. Matsunami, J. Cryst. Growth **78**, 538 (1986).

[29] P. Pirouz, C. M. Chorey, and J. A. Powell, Appl. Phys. Lett. **50**, 221 (1987).

[30] H. S. Kong, Y. C. Wang, J. T. Glass, and R. F. Davis, J. Mater. Res. **3**, 521 (1988).

[31] M. Kitabatake and J. E. Greene, Jpn. J. Appl. Phys. 1 **35**, 5261 (1996).

[32] J. Stoemenos, C. Dezauzier, G. Arnaud, S. Contreras, J. Camassel, J. Pascual, and J. L. Robert, Mater. Sci. Eng. B **29**, 160 (1995).

[33] M. Diani, J. L. Bischoff, L. Kubler, and D. Bolmont, Appl. Surf. Sci. **68**, 575 (1993).

[34] R. L. Summers (unpublished).

[35] A temperature of 300 K is used since in the pressure range of interest the gas molecule collide much more frequently with the walls of the vacuum chamber than with the hot substrate. For C_2H_2, Q (in molecules/cm^2) $=3.98\times10^{14}\times L$ where L is the exposure in Langmuirs.

[36] S. Juillaguet, L. Kubler, M. Diani, J. L. Bischoff, G. Gewinner, P. Wetzel, and N. Bécourt, Surf. Sci. **339**, 363 (1995).

[37] D. A. Shirley, Phys. Rev. B **5**, 4709 (1972).

[38] R. Nyholm and N. Mårtensson, Chem. Phys. Lett. **74**, 337 (1980).

[39] K. Hricovini, R. Günther, P. Thiry, A. Taleb-Ibrahimi, G. Indlekofer, J. E. Bonnet, P. Dumas, Y. Petroff, X. Blase, Xuejun Zhu, Steven G. Louie, Y. J. Chabal, and P. A. Thiry, Phys. Rev. Lett. **70**, 1992 (1993).

[40] M. P. Seah and W. A. Dench, Surf. Interface Anal. **1**, 2 (1979).

[41] V. Quillet, F. Abel, and M. Schott, Nucl. Instrum. Methods Phys. Res. Sect. B **83**, 47 (1993).

[42] D. Dieumegard, D. Dubreuil, and G. Amsel, Nucl. Instrum. Methods **166**, 431 (1979).

[43] J. Graul and E. Wagner, Appl. Phys. Lett. **21**, 67 (1972). According to these authors, the parabolic constant is equal to $2N_0a^3D$, where N_0 is the concentration of silicon at the interface (5×10^{22} cm^{-3}), a^3 is $\frac{1}{4}$ of the volume of the $3C$-SiC unit cell ($a=4.36$ Å), and D is the diffusion coefficient.

[44] We recall that the surface density of a (001) atomic layer is 6.8×10^{14} atoms/cm^2 in Si and 10.5×10^{14} atoms/cm^2 in $3C$-SiC.

[45] T. L. Barr and S. Seal, J. Vac. Sci. Technol. A **13**, 1239 (1995).

[46] A. T. S. Wee, Z. C. Feng, H. H. Hng, K. L. Tan, C. C. Tin, R. Hu, and R. Coston, Appl. Surf. Sci. **81**, 377 (1994).

[47] R. Kaplan, Surf. Sci. **215**, 111 (1989).

[48] V. M. Bermudez, J. Appl. Phys. **63**, 4951 (1988), and references therein.

[49] An application of the continuous overlayer model with escape depth of Si $2p$ photoelectrons in SiC and Si of about 20 Å would lead to an estimated XPS thickness of about 55 Å for $Q\sim6\times10^{18}$ molecules/cm^2.

[50] M. Riehl-Chudoba, P. Soukiassian, C. Jaussaud, and S. Dupont, Phys. Rev. B **51**, 14 300 (1995).

[51] L. Pauling, *The Nature of the Chemical Bond*, 2nd ed. (Cornell University Press, Ithaca, NY, 1945).

[52] L. I. Johansson and I. Lindau, Solid State Commun. **36**, 695 (1980).
[53] E. A. Kraut, R. W. Grant, J. R. Waldrop, and S. P. Kowalczyk, Phys. Rev. Lett. **44**, 1620 (1980).
[54] J. Robertson, J. Non-Cryst. Solids **97/98**, 863 (1987).
[55] R. C. Fang and L. Ley, Phys. Rev. B **40**, 3818 (1989).
[56] C. S. Fadley, Phys. Scr. **T17**, 39 (1987).
[57] C. S. Fadley, in *Synchrotron Radiation Research: Advances in Surface Science*, edited by Z. Bachrach (Plenum, New York, 1990), and references therein.
[58] H. C. Poon and S. Y. Tong, Phys. Rev. B **30**, 6211 (1984).
[59] X. Chen, T. Abukawa, J. Tani, and S. Kono, Phys. Rev. B **52**, 12 380 (1995).
[60] J. J. Rehr and R. C. Albers, Phys. Rev. B **41**, 8139 (1990).
[61] D. Agliz, A. Quémerais, and D. Sébilleau, Surf. Sci. **343**, 80 (1995).
[62] T. A. Tyson, K. O. Hodgson, C. R. Natoli, and M. Benfatto, Phys. Rev. B **46**, 5997 (1992).
[63] A. P. Kaduwela, D. J. Friedmann, and C. S. Fadley, J. Electron Spectrosc. Relat. Phenom. **57**, 223 (1991).
[64] H. Rücker, M. Methfessel, E. Bugiel, and H. J. Osten, Phys. Rev. Lett. **72**, 3578 (1994).